



1 Permafrost-wildfire interactions: Active layer thickness estimates for 2 paired burned and unburned sites in northern high-latitudes

3 Anna C. Talucci¹, Michael M. Loranty², Jean E. Holloway³, Brendan M. Rogers¹, Heather D.
4 Alexander⁴, Natalie Baillargeon¹, Jennifer L. Baltzer⁵, Logan T. Berner⁶, Amy Breen⁷, Leya Brodt⁸,
5 Brian Buma^{9, 10}, Jacqueline Dean¹, Clement J. F. Delcourt¹¹, Lucas R. Diaz¹¹, Catherine M. Dieleman¹²,
6 Thomas A. Douglas¹³, Gerald V. Frost¹⁴, Benjamin V. Gaglioti¹⁵, Rebecca E. Hewitt¹⁶, Teresa
7 Hollingsworth^{17, 18}, M. Torre Jorgenson¹⁹, Mark J. Lara²⁰, Rachel A. Loehman²¹, Michelle C. Mack²²,
8 Kristen L. Manies²³, Christina Minions¹, Susan M. Natali¹, Jonathan A. O'Donnell²⁴, David Olefeldt²⁵,
9 Alison K. Paulson²⁶, Adrian V. Rocha²⁷, Lisa B. Saperstein²⁸, Tatiana A. Shestakova^{29, 30, 1}, Seeta
10 Sistla³¹, Oleg Sizov³², Andrey Soromotin⁸, Merritt R. Turetsky³³, Sander Veraverbeke¹¹, Michelle A.
11 Walvoord³⁴

- 12
13 ¹ Woodwell Climate Research Center, Falmouth, MA, 02540-1644, USA
14 ² Department of Geography, Colgate University, Hamilton, NY, 13346, USA
15 ³ Department of Geography, Environment and Geomatics, University of Ottawa, Ottawa, K1N 6N5, Canada
16 ⁴ College of Forestry, Wildlife, and Environment, Auburn University, Auburn, AL, 36949, USA
17 ⁵ Biology Department, Wilfrid Laurier University, Waterloo, ON, N2L 3C5, Canada
18 ⁶ School of Informatics, Computing, and Cyber Systems, Northern Arizona University, Flagstaff, AZ, 86011, USA
19 ⁷ International Arctic Research Center, University of Alaska Fairbanks, Fairbanks, AK, 99775-7340, USA
20 ⁸ Tyumen State University, Tyumen, 625003, Russia
21 ⁹ Integrative Biology, University of Colorado (Denver), Boulder, CO, 80304, USA
22 ¹⁰ Environmental Defense Fund, Boulder, CO 80302, USA
23 ¹¹ Faculty of Science, Vrije Universiteit Amsterdam, Amsterdam, 1081 HV, The Netherlands
24 ¹² School of Environmental Sciences, University of Guelph, Guelph, ON, N3H3Y8, Canada
25 ¹³ U.S. Army Cold Regions Research and Engineering Laboratory, Fort Wainwright, AK, 99703, USA
26 ¹⁴ Alaska Biological Research, Inc., Fairbanks, AK, 99708, USA
27 ¹⁵ Water and Environmental Research Center, University of Alaska Fairbanks, Fairbanks, AK, 99775, USA
28 ¹⁶ Department of Environmental Studies, Amherst College, Amherst, MA, 01002, USA
29 ¹⁷ Pacific Northwest Research Station, USDA Forest Service, University of Alaska Fairbanks, Fairbanks, AK, 99708, USA
30 ¹⁸ Aldo Leopold Wilderness Research Institute, Rocky Mountain Research Station, Missoula MT, 59801
31 ¹⁹ Alaska Ecoscience, Fairbanks, AK, 99775, USA
32 ²⁰ Department(s) of Plant Biology and Geography, University of Illinois Urbana-Champaign, Urbana, IL, 61801, USA
33 ²¹ U.S. Geological Survey, Alaska Science Center, Anchorage, AK, 99508, USA
34 ²² Center for Ecosystem Science and Society and Department of Biological Sciences, Northern Arizona University, Flagstaff,
35 AZ, 86001, USA
36 ²³ U.S. Geological Survey, Moffett Field, 94035, USA
37 ²⁴ Arctic Network, National Park Service, Anchorage, AK, 99501, USA
38 ²⁵ Department of Renewable Resources, University of Alberta, Edmonton, AB, T6G 2G7, Canada
39 ²⁶ Humboldt-Toiyabe National Forest, U.S. Forest Service, Sparks, NV, 89431, USA
40 ²⁷ Department of Biological Sciences, University of Notre Dame, Notre Dame, IN, 46556, USA
41 ²⁸ Alaska Regional Office, U.S. Fish and Wildlife Service, Anchorage, AK, 99503, USA
42 ²⁹ Department of Agricultural and Forest Sciences and Engineering, University of Lleida, Av. Alcalde Rovira Roure 191,
43 Lleida, Catalonia 25198, Spain



- 44 ³⁰ Joint Research Unit CTFC–AGROTECNIO–CERCA, Av. Alcalde Rovira Roure 191, Lleida, Catalonia 25198, Spain
45 ³¹ Natural Resources Management & Environmental Sciences, Cal Poly, San Luis Obispo, CA, 93401, USA
46 ³² Oil and Gas Research Institute RAS, Moscow, 119333, Russia
47 ³³ Renewable and Sustainable Energy Institute, Department of Ecology and Evolutionary Biology, University of Colorado
48 Boulder, Boulder, CO, 80309-0552, USA
49 ³⁴ U.S. Geological Survey, Earth System Processes Division, Denver, CO, 80225, USA
50

51 *Correspondence to:* Anna C. Talucci (atalucci@woodwellclimate.org)

52
53

54

55 **Abstract.** As the northern high latitude permafrost zone experiences accelerated warming, permafrost has become vulnerable
56 to widespread thaw. Simultaneously, wildfire activity across northern boreal forest and Arctic/subarctic tundra regions impact
57 permafrost stability through the combustion of insulating organic matter, vegetation and post-fire changes in albedo. Efforts
58 to synthesise the impacts of wildfire on permafrost are limited and are typically reliant on antecedent pre-fire conditions. To
59 address this, we created the FireALT dataset by soliciting data contributions that included thaw depth measurements, site
60 conditions, and fire event details with paired measurements at environmentally comparable burned and unburned sites. The
61 solicitation resulted in 52,466 thaw depth measurements from 18 contributors across North America and Russia. Because thaw
62 depths were taken at various times throughout the thawing season, we also estimated end of season active layer thickness
63 (ALT) for each measurement using a modified version of the Stefan equation. Here, we describe our methods for collecting
64 and quality checking the data, estimating ALT, the data structure, strengths and limitations, and future research opportunities.
65 The final dataset includes 47,952 ALT estimates (27,747 burned, 20,205 unburned) with 32 attributes. There are 193 unique
66 paired burned/unburned sites spread across 12 ecozones that span Canada, Russia, and the United States. The data span fire
67 events from 1900 to 2022. Time since fire ranges from zero to 114 years. The FireALT dataset addresses a key challenge: the
68 ability to assess impacts of wildfire on ALT when measurements are taken at various times throughout the thaw season
69 depending on the time of field campaigns (typically June through August) by estimating ALT at the end of season maximum.
70 This dataset can be used to address understudied research areas particularly algorithm development, calibration, and validation
71 for evolving process-based models as well as extrapolating across space and time, which could elucidate permafrost-wildfire
72 interactions under accelerated warming across the high northern latitude permafrost zone. The FireALT dataset is available
73 through the Arctic Data Center.
74

75

76

77 **1 Introduction**

78 Permafrost, defined as ground that remains at or below 0°C for two or more consecutive years, has become vulnerable to
79 widespread thaw in response to rapid climate warming at high latitudes. Permafrost temperatures have increased over the last
80 30 years (Romanovsky et al., 2010, Smith et al., 2022, Calvin et al., 2023) resulting in the thickening of the active layer, which
81 is the uppermost, seasonally thawed layer (Harris and Permafrost Subcommittee, Associate Committee on Geotechnical
82 Research, National Research Council of Canada, 1988, Bonnaventure and Lamoureux 2013). Widespread permafrost thaw and



83 increases in active layer thickness are expected under future climate conditions (Smith and Burgess 2004, Zhang et al., 2008,
84 Derksen et al., 2019, Peng et al., 2023), and these processes are expected to release large amounts of soil carbon to the
85 atmosphere as greenhouse gas emissions (Schaefer et al., 2014, Gasser et al., 2018, Knoblauch et al., 2018, Yokohata et al.,
86 2020, Natali et al., 2021, Schuur et al., 2022, See et al., 2024). Changes to permafrost, particularly near-surface permafrost
87 and the active layer, have important implications for ecology, forestry, hydrology, biogeochemistry, climate feedbacks,
88 engineering, traditional livelihoods, and community safety (Anisimov and Reneva 2006, O'Donnell et al., 2011b, Rocha and
89 Shaver 2011, Bret-Harte et al., 2013, Hugelius et al., 2014, Jones et al., 2015, Li et al., 2019, Turetsky et al., 2020, Gibson et
90 al., 2021, Huang et al., 2024).

91
92 Climate change is also intensifying high-latitude wildfire regimes (Kasischke et al., 2010, de Groot et al., 2013, Zhang et al.,
93 2015, Wotton et al., 2017, Hanes et al., 2019, McCarty et al., 2021, Descals et al., 2022, Phillips et al., 2022, Scholten et al.,
94 2022, Zheng et al., 2023, Byrne et al., 2024). Wildfire activity shows interannual variability that is predominantly controlled
95 by subseasonal drying and climate, where prolonged warm and dry conditions in conjunction with fuel accumulation may alter
96 fire regimes and the seasonality of fire (York et al., 2020). The interaction between wildfire and permafrost results in both
97 immediate and long-term effects on the surface energy balance and ground thermal regimes, as well as hydrologic cycling and
98 soil and aquatic biogeochemistry (O'Donnell et al., 2011b, Rocha and Shaver 2011, Bret-Harte et al., 2013, Jones et al., 2015,
99 Li et al., 2019, Hollingsworth et al., 2020, Holloway et al., 2020). These interactions also result in second-order greenhouse
100 gas emissions (O'Donnell et al., 2011c, Jiang et al., 2015, Smith et al., 2015, Jones et al., 2015, Gibson et al., 2018, Li et al.,
101 2019) by making stored soil carbon available for mineralization (O'Donnell et al., 2011c, Rocha and Shaver 2011, Bret-Harte
102 et al., 2013, Hugelius et al., 2014, Jones et al., 2015, Li et al. 2019). Biomass combustion during fires removes the insulating
103 surface vegetation (i.e., moss, lichen, low growing shrubs) and soil organic matter, typically reduces evapotranspiration (Rouse
104 1976, Amiro 2001, Chambers and Chapin 2002, Chambers et al., 2005, Amiro et al., 2006), and reduces short-term albedo
105 (i.e., the surface reflectance), resulting in increases in the ground heat flux and the expansion of the active layer (Rocha et al.,
106 2012, Jafarov et al., 2013, Nosssov et al., 2013, Jiang et al., 2015, Douglas et al., 2016, Fisher et al., 2016, Gibson et al., 2018).
107 Similarly, tree canopy removal reduces shading in the summer and results in more snow on the ground in the winter, both
108 leading to higher surface soil temperatures and expansion of the active layer into near-surface permafrost (Rocha et al., 2012,
109 Jafarov et al., 2013, Jiang et al., 2015, Zhang et al., 2015, Douglas et al., 2016, Fisher et al., 2016, Gibson et al., 2018). In
110 contrast, across Arctic tundra, shrub removal from wildfire results in thinner snow due to increased wind exposure, which
111 causes a reduction of the active layer (Wang et al., 2012, Jones et al., 2024).

112
113 Post-fire changes in the energy balance and subsequent increases in the active layer thickness have historically recovered to
114 pre-fire conditions as vegetation succession occurred (Rouse 1976, Amiro 2001, Liu et al., 2005, Amiro et al., 2006), with a
115 maximum active layer thickness often observed 5-10 years post-fire (Rocha et al., 2012, Holloway et al., 2020) but may extend
116 up to 30 years post-fire (Gibson et al., 2018). However, this pattern of recovery may be changing alongside climate warming



117 and shifting fire regimes (Brown et al., 2015), and may be further impacted by secondary disturbances (Hayes and Buma,
118 2021). For example, as wildfire burns across permafrost peatlands, not only is there a thicker and warmer active layer but an
119 expansion of year-round unfrozen ground (i.e., taliks) and thermokarst bogs (Gibson et al., 2018). These changes in active
120 layer thickness and hydrologic dynamics can constrain regeneration by prolonging vegetation recovery and inducing shifts in
121 vegetation composition and structure (Baltzer et al., 2014, Dearborn et al., 2021). Further, near-surface permafrost degradation
122 can lead to ground subsidence, which alters surface hydrology, often leading to water inundation and further degradation
123 (Brown et al., 2015). Where wildfires burn across permafrost landforms (e.g., thermokarst, ice rich areas), deep and irreversible
124 thawing could permanently alter the landscape (Burn and Lewkowitz 1990, Lewkowitz 2007, Sannel and Kuhry 2011,
125 Liljedahl et al., 2016, Rudy et al., 2017, Borge et al., 2017, Mamet et al., 2017, Fraser et al., 2018), releasing long stored soil
126 carbon into the atmosphere (Schuur et al., 2015). Currently, emissions from fire-induced permafrost thaw are underestimated
127 by the scientific community and climate models (Natali et al., 2021, Treharne et al., 2022, Schädel et al., 2024), an issue that
128 is exacerbated by modelling challenges and uncertainties associated with permafrost carbon stocks (Hugelius et al., 2014,
129 Turetsky et al., 2020). The change in active layer thickness over time is a critical diagnostic indicator of permafrost conditions
130 (Brown et al., 2000, Shiklomanov et al., 2010) and a vital component of modelling carbon emissions from fire and non-fire
131 related permafrost thaw.

132
133 To provide critical data that can be used for understanding and modelling impacts of wildfire on permafrost, we compiled a
134 dataset of thaw depth measurements from paired burned and unburned sites across the northern high-latitude permafrost zone.
135 This dataset is the first of its kind to focus on paired burned and unburned sites providing a circumpolar/boreal perspective.
136 Climate and ecosystem conditions including drainage, vegetation, and soil characteristics control near-surface permafrost
137 characteristics, and thus in order to detect an influence of wildfire it is necessary to have measurements either pre- and post-
138 fire, or unburned control and burned nearby sites with otherwise similar ecosystem properties. Measuring ALT for paired
139 unburned control and nearby burn sites is more realistic due to the stochasticity of wildfire. Further, unburned control sites
140 provide a benchmark for understanding the impact of wildfire in these dynamic systems. Thaw depth increases over the course
141 of the thawing season until it reaches its maximum depth, i.e., active layer thickness (ALT). This means that early to mid-
142 season measurements do not capture the full depth of the thawed active layer. As such, the variability in thawing season and
143 measurement timing makes it difficult to compare across space and time. Therefore, we standardised thaw depths taken at
144 different times throughout the thawing season, which resulted in an estimated dataset of ALT. Further, capturing the maximum
145 ALT aids in establishing the full scope of permafrost change because it is a critical indicator of thaw dynamics. Depending on
146 the location ALT could occur anywhere from August through November. This paper provides a description of the data
147 solicitation and compilation, the process for standardising the measurements, and general descriptive statistics on the dataset.
148 Finally, we describe the strengths and limitations of the dataset, future research directions, and protocols for accessing and
149 using this dataset.

150



151 **2 Data and Methods**

152 **2.1 Data Solicitation and Quality Screening**

153 To assemble a dataset capable of widely characterising the influence of wildfire on permafrost, we solicited field measurements
 154 of thaw depth from paired burned and unburned sites from researchers working in boreal forest and tundra ecosystems. Thaw
 155 depth refers to depth or thickness of the unfrozen surface soil layer anytime during the thawing season, and is typically obtained
 156 by measuring depth to refusal using a graduated steel probe. A critical component of the data required an ecologically
 157 appropriate unburned site(s) within close proximity that shared similar dominant vegetation, drainage, and climatic conditions
 158 to be paired with one or more burned sites, meaning the burned site would have had similar pre-fire conditions to the unburned
 159 site. We began by soliciting data from members of the Permafrost Carbon Network and their collaborators and then used
 160 literature review to identify additional contributors. Data contributors were required to submit metadata (Table S1) and data
 161 via a Google form with required attributes that included their last name, country where data were collected, latitude, longitude,
 162 biome, vegetation cover class, site identifier, plot identifier, year data were collected, month data were collected, day data was
 163 collected, fire identifier, fire year, whether the site was burned or unburned, organic layer depth, thaw depth, whether the probe
 164 hit rocks, whether the depth was greater than the probe, contributors assigned a designation of ‘thaw’ or ‘active’ to indicate
 165 early-mid or late season measurements respectively, slope, topographic position, pairing, and whether surface water was
 166 present. The solicitation resulted in the contribution of 18 datasets with 52,466 thaw depth measurements covering portions of
 167 the northern high-latitude permafrost zones in Canada, Russia, and the United States (Table 1, Fig. 1).

169 **Table 1. Brief description of the data contributions. Table includes the last name of the contributor, geographic location of the data,**
 170 **fire years that were sampled and relevant citations associated with the data.**

Contributor	Country	Location description	Biome	Ecozone	Fire years	Citations
Baillargeon	United States	Yukon Kuskokwim Delta, AK, USA	Tundra	Beringia lowland tundra	1972, 2015	Baillargeon et al., 2022
Breen	United States	Kougarok Tundra fire complex on the Seward Peninsula, AK, USA	Tundra	Beringia upland tundra	1971, 1982, 2002, 2011	Hollingsworth et al., 2020, 2021
Buma	United States	Central Alaska black spruce forest	Boreal	Interior Alaska-Yukon lowland taiga	2005	B. Buma, University of Colorado (Denver), unpublished data, 2005
Delcourt	Russia	Northeast Siberia, Russia	Boreal	East Siberian taiga	2018	Delcourt et al., 2024
Diaz	United States	Alaska, USA	Boreal; Tundra	Interior Alaska-Yukon lowland taiga; Beringia lowland tundra	2022	L.R. Diaz, Vrije Universiteit Amsterdam, unpublished data, 2022



Baltzer, Dieleman, Turetsky	Canada	Northwest Territories, Canada	Boreal	Muskwa-Slave Lake taiga; Northern Canadian Shield taiga; Northwest Territories taiga	1940, 1960, 1969, 1971, 1972, 1973, 1980, 1981, 2011, 2013, 2014	Dieleman et al., 2022
Douglas, Jorgenson	United States	Interior Boreal near Fairbanks, AK, USA	Boreal	Interior Alaska-Yukon lowland taiga	2005-2020	Douglas et al., 2020
Frost	United States	central Yukon-Kuskokwim Delta, western Alaska	Tundra	Beringia lowland tundra	1971, 1972, 1985, 2006, 2007, 2015	Frost et al., 2020
Gaglioti	United States	The Noatak watershed, which drains the southwestern flank of the Brooks Range in northwestern Alaska	Tundra	Arctic foothills tundra	1972, 1984	Gaglioti et al., 2021
Holloway	Canada	Taiga Plains and Taiga Shield ecozones near Yellowknife, Canada	Boreal	Muskwa-Slave Lake taiga; Northern Canadian Shield taiga; Northwest Territories taiga	2014, 2015	Holloway et al., 2024
Loranty	Russia	Northeastern Siberia Larch forests	Tundra	Chukchi Peninsula tundra	1972	Loranty, et al., 2014
Manies	United States	Interior Alaska, black spruce forests	Boreal	Interior Alaska-Yukon lowland taiga	1999	Harden et al., 2006
Natali	United States	Bonanza Creek, Alaska USA; Anaktuvuk River fire, AK USA; Yukon Kuskokwim Delta, AK	Boreal; Tundra	Interior Alaska-Yukon lowland taiga; Interior Yukon-Alaska alpine tundra; Arctic foothills tundra; Beringia lowland tundra	1983, 2003, 2004, 2007, 2015	Natali et al., 2016, 2018, Natali 2018
O'Donnell	United States	Interior Boreal, AK, USA	Boreal; Tundra	Interior Alaska-Yukon lowland taiga; Interior Yukon-Alaska alpine tundra	1966, 1967, 1990, 2003, 2004	O'Donnell et al., 2009, 2011a, 2011b, 2013
Olefeldt	Canada	Western Boreal Canada	Boreal	Muskwa-Slave Lake taiga; Northwest Territories taiga	1964, 1967, 1975, 1982, 1984, 1995, 2000, 2006, 2007, 2008, 2012, 2013, 2014, 2019	Gibson et al., 2018
Paulson, Alexander	Russia	Northeastern Siberia near Cherskiy, Russia, and Yakutsk, Russia	Boreal	East Siberian taiga; Northeast Siberian taiga	1983, 1984, 1990, 2001, 2002, 2003, 2010, 2015	Alexander et al., 2020
Rocha	United States	North Slope of Alaska	Tundra	Arctic foothills tundra	1977, 1993, 2001, 2007	Rocha and Shaver, 2011
Sizov	Russia	Northwestern Russia, Nadym region of the Yamal-Nenets Autonomous Okrug	Tundra	Yamal-Gydan tundra	2016	Sizov et al., 2020



172
 173 **Figure 1. Map of the northern high latitude permafrost zone showing the percent of thaw depth measurements by ecozones (circle**
 174 **colour, Dinerstein et al., 2017) with the extent of continuous, discontinuous, and sporadic permafrost shown in shades of blue (Brown**
 175 **et al., 1998). Points are sized and labelled with the percent of measurements within each ecozone. The Arctic circle is shown with the**
 176 **thick dashed black line.**

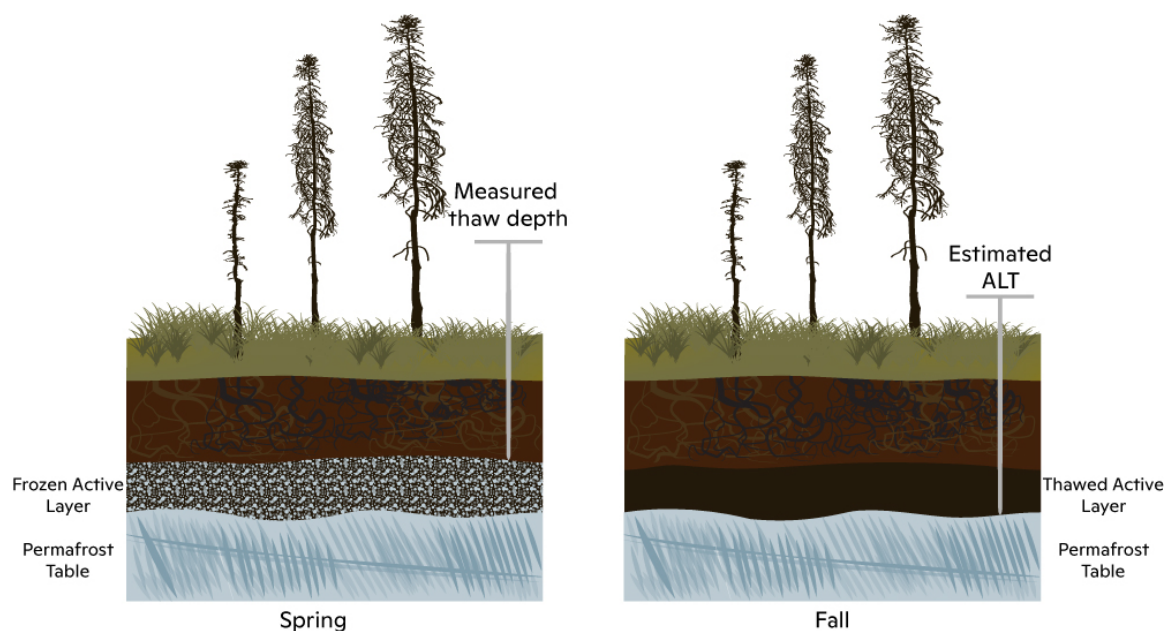
177



178 We screened the data for issues with units, sign convention, coordinates, and data type (e.g., factor, integer). Where we required
179 categorical variables, we ensured these were spelled in a consistent manner and that the correct unique number of variables
180 were returned. We mapped the data to check inaccurate site coordinates and checked discrepancies, such as missing negative
181 signs from longitude, with contributors. We used histograms of measurement depths to identify any outliers in the data, several
182 of which were removed after confirming with the contributors that they were the result of topographic errors. Data contributors
183 were asked to note if any measurements hit rock, and, when noted, these observations were excluded from the final dataset.
184

185 2.2 Estimating Active Layer Thickness

186 Over the course of the growing season, the depth of the thawing front increases as the active layer expands to its maximum.
187 Therefore, measurements taken throughout the thaw season are not directly comparable with one another. Therefore, we
188 standardised thaw depths taken at different times throughout the thawing season, which resulted in an estimated dataset of
189 ALT. To do so, we estimated ALT using a modified version of the Stefan equation, used by Holloway and Lewkowicz (2020)
190 and described by Riseborough et al. (2018) and Bonnaventure and Lamoureux (2013). Estimating ALT (Fig. 2) allows thaw
191 depth measurements collected during different times in the growing season to be comparable and used to understand the full
192 effects of wildfire on the active layer across paired sites in a given measurement year and for some of the sites across multiple
193 years.



194

195 **Figure 2. Diagram of early season thaw depth measurement versus late season active layer thickness. The active layer expands**
196 **during the thawing season reaching its maximum thickness between August and November depending on the location.**



197 ALT was estimated based on air thawing degree days (TDD; i.e., days above zero degrees Celsius during the thawing season).
198 Daily mean air temperatures were extracted from ERA5-Land daily aggregates (Muñoz Sabater 2019) accessed through
199 Google Earth Engine (Gorelick et al., 2017). Instrumental air temperature data are sparse across the northern high-latitude
200 regions. We selected the ERA5-Land (Muñoz Sabater, 2019) dataset since it is available for the full region and time series,
201 accessible through Google Earth Engine, and has been evaluated against meteorological station data (Rantanen et al., 2023,
202 Clelland et al. 2024). Across the circum-Arctic and Asian boreal ERA5-Land validation studies indicate a warming bias in
203 winter months of a half a degree Celsius (Rantanen et al., 2023, Clelland et al. 2024), whereas validation studies in summer
204 indicate a slight cooling trend of ~0.2 degrees Celsius (Rantanen et al., 2023). Due to the scarcity of meteorological stations
205 across the Northwestern Territories, we provide additional validation for air temperature data from ERA5-Land using shielded
206 air temperatures at a height of 1.5 m that were measured at six sites using Onset Corporation (USA) Hobo Pro U23-003 loggers
207 (accuracy ±0.21°C; precision ±0.02°C). All air temperature data were aggregated from 2-hour samples to daily averages and
208 sites included thaw depth measurements (Holloway 2020). We calculate Pearson’s correlation coefficient (R), bias (defined as
209 the summation of modelled minus measured divided by the number of data points), and the root mean square error (RMSE).
210 The correlation is ~0.99, with a warming bias of 0.54 degrees Celsius, and a RMSE of 2.23 degrees Celsius (Fig. S2).

211
212 First, we defined the end of the thaw season for each measurement location and year based on when the five-day mean daily
213 air temperature shifted from above- to below-freezing. We then subtracted 14 days from the end-of-season date to account for
214 the lag between surface freezing and the refreezing of the bottom of the active layer. Typically, the active layer begins to freeze
215 upward while the air temperature is still above zero, requiring approximately 7-14 days until the surface freezes (Osterkamp
216 and Burn 2002). Following the Stefan equation (Freitag and McFadden, 1997), we calculate (A) as the square root of the sum
217 of daily mean air temperature TDD prior to the day of year of the field measurement (i.e., thaw depth), as in Eq. (1):

$$218 \quad A = \sqrt{\sum_{TDD \text{ thaw depth}=1}^n TDD \text{ Thaw depth}}, \quad (1)$$

220
221 We calculate (B) as the square root of the sum of daily mean air temperature TDD (i.e., days above zero degrees Celsius) prior
222 to the end of thaw season day of year (i.e., ALT) Eq. (2):

$$223 \quad B = \sqrt{\sum_{TDD \text{ ALT}=1}^n TDD \text{ ALT}}, \quad (2)$$

225
226 Finally, we multiplied the field measured depth by the ratio of the first two equations to calculate the estimated ALT Eq. (3):

227

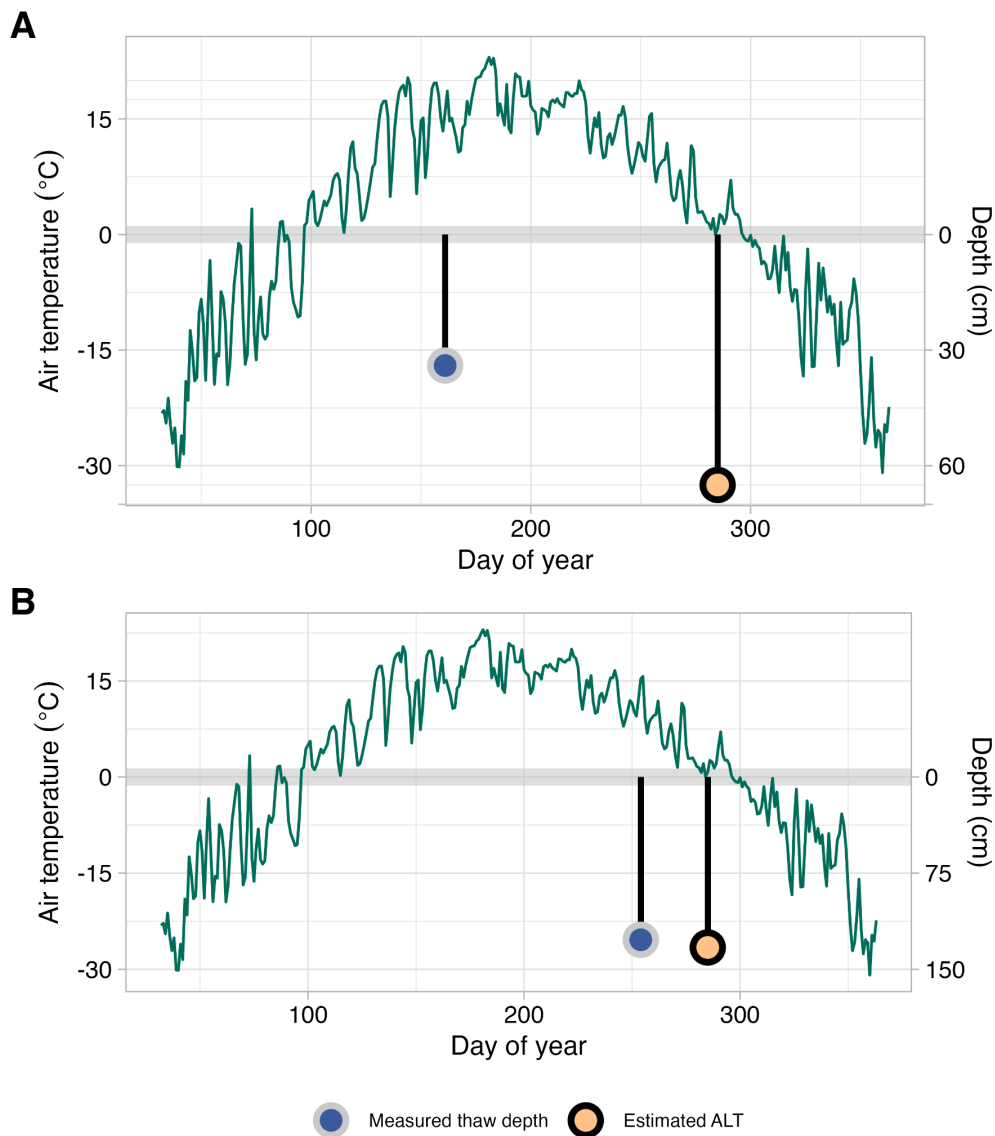


228 $estimated\ ALT = field\ measured\ depth \times (B \div A),$ (3)

229

230 An example of the calculation for two sites is provided in Table 3 and shown in Fig. 3.

231



232

233 **Figure 3.** An example of estimating active layer thickness from two *in situ* thaw depth measurements using seasonal air temperature.
234 Air temperature through the thawing season (green line) for two separate sites, one with an early-season thaw depth measurement
235 (A) and a second with an end-of-season thaw depth measurement (B). For each site, we show the measured thaw depth (blue point)
236 and estimated ALT depth (orange point) for the day of year either measured or estimated. The right y-axis shows thaw depth (cm),
237 the left y-axis shows air temperature and the x-axis shows the day of the year.



238
 239

Table 3. An example of estimating ALT using Equations 1-3 from two *in situ* thaw depth measurements at two sites (A and B) using the same data as in Fig. 3.

	Site	A	B
Data contribution	Timing of measurement	Early season	End of Season
	Year	2015	2015
	Month	6	9
	Day	10	11
	Day of year	161	254
	Measurement depth (cm)	34	127
Calculated from ERA5 data extracted based on location	Day of year first of five consecutive days at zero	299	299
	Day of year to estimate ALT	285	285
	Eq.1	25.25	45.95
	Eq.2	48.03	48.03
Estimated ALT	Eq.3 (cm)	65	133

240

241 Estimates were excluded for observations that hit rock, were greater than the depth of the measurement probe, or were missing
 242 the day of month (Table S2). We were unable to convert every early season thaw depth to ALT if the date of measurement
 243 was not preceded by at least one day above zero degrees Celsius, in which case these measurements were removed from the
 244 estimated dataset. Ultimately, 47,952 of the original 52,466 measurements were included in the estimated dataset.

245

246 2.3 Quantify uncertainty of estimated ALT

247 We quantify uncertainty in our estimates of ALT by calculating Pearson’s correlation coefficient (R), bias (defined as the
 248 summation of modelled minus measured divided by the number of data points), and the Root Mean Square Error (RMSE). The
 249 bias indicates whether estimated ALT is over or underestimated, while the RMSE provides an average error regardless of sign.
 250 We used a separate dataset ($n=626$) that had repeat thaw depth measurements at the same location taken throughout the thaw
 251 season. We used the early season measurements to estimate thaw depths for the date of the late season measurement (as
 252 opposed to the end of the thaw season defined using ERA5-Land) following the methodology described in Section 2.2, to
 253 quantify the uncertainty in the estimation process.

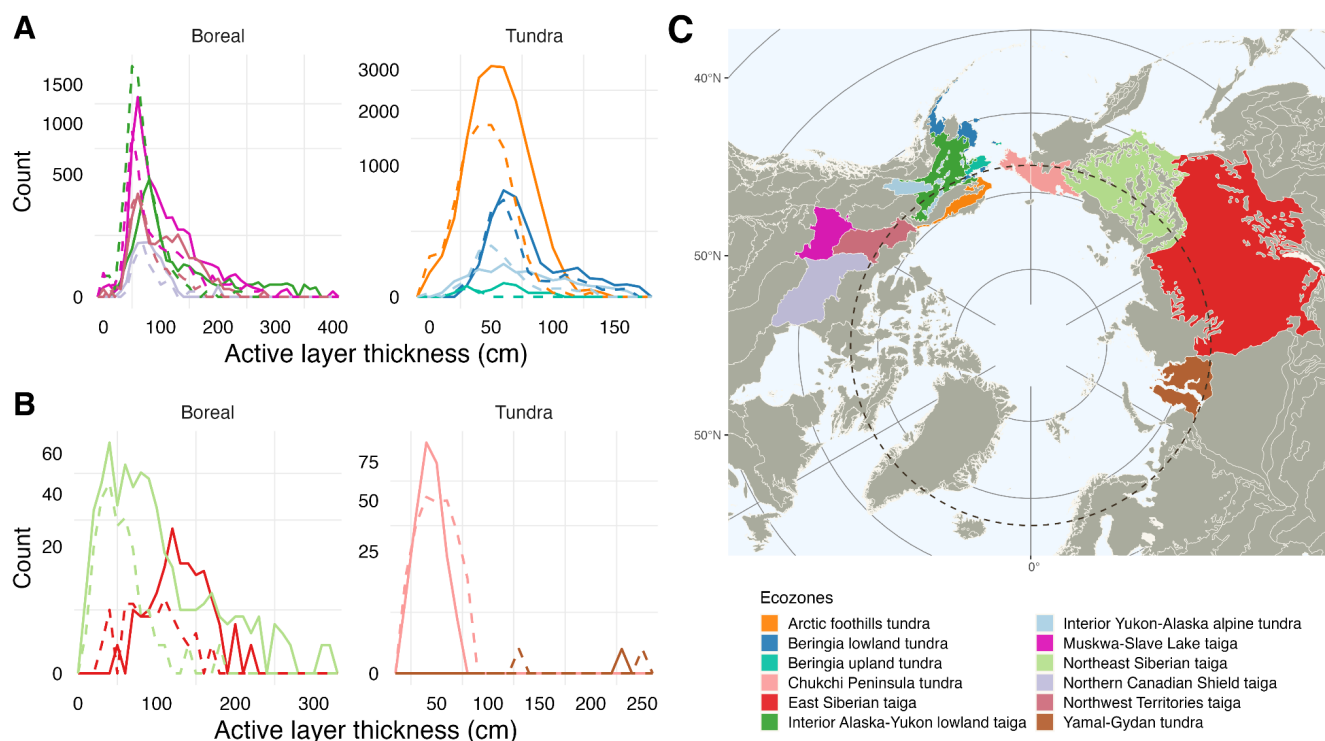
254 2.4 Spatial attributes

255 We added spatial attributes to the data through spatial joins. We generated a point shapefile using the latitude and longitude
 256 coordinates with the coordinate reference system (CRS) 4326 (i.e., WGS 84). We performed a spatial join to add ecozone data
 257 (Dinerstein et al., 2017), retaining the ecozone and biome names. We then performed a second spatial join with permafrost
 258 data (Brown et al., 1998), retaining permafrost extent (e.g., continuous, discontinuous, sporadic). We show the distribution of
 259 estimated ALT measurements by ecozone (Fig. 4).

260



261



262

263 **Figure 4.** Frequency distribution graphs showing estimated active layer thickness (cm) by ecozones split by North America (A) and
 264 Eurasia (B). Map of ecozones for location reference (C; Dinerstein et al., 2017). The y-axis is the count of measurements and the x-
 265 axis is the depth in centimetres. Both x- and y-axis vary by panel and y-axes are adjusted to show low counts.

266 2.5 Data structure and columns

267 The resulting dataset includes 32 attributes including attributes from the initial contribution, plus the attributes from the spatial
 268 joins and the derived ALT estimates all described in Table 4. The dataset is shared in comma separated values (csv) format
 269 with 47,952 rows and 32 columns. For missing values, we used ‘NA’ and ‘-9999’, for character and numeric fields,
 270 respectively.

271

272 **Table 4.** Description of data attributes and data format.

Attribute	Format	Description
plotId	character	A unique identifier assigned by the data contributor to identify the field plot.
siteId	character	Site name assigned by the data contributor specific to the fieldwork.
lastNm	character	Last name(s) of the person(s) contributing the data provided by the data contributor.
submitNm	character	Last name of the data contributor that submitted the form (single name only).
biome	character	Boreal (B) or tundra (T) assigned by the data contributor.



distur	character	Categorical variable to identify location as burned or unburned provided by the data contributor.
cntryId	character	Dropdown list of two-digit code: Russia (RU), USA (US), Canada (CA), Finland (FI), Norway (NO), Sweden (SE), Iceland (IS), Greenland (GL) assigned by the data contributor.
fireYr	integer	Four-digit year of when the fire event occurred provided by the data contributor.
fireId	character	Unique fire identifier assigned by the data contributor.
gtProbe	character	Permafrost thaw depth exceeds (i.e., greater than [gt]) the length of probe yes (y) or no (n) provided by the data contributor.
hitRock	character	Probe hit rock yes (y) or no (n) provided by the data contributor.
lat	float	Latitude in decimal degrees in WGS 84 provided by the data contributor.
lon	float	Longitude in decimal degrees in WGS 84 provided by the data contributor.
year	integer	Four-digit year the data were collected provided by the data contributor.
month	integer	Two-digit month (values 01-12 accepted) the data were collected provided by the data contributor.
day	integer	Day of month data were collected values(1-31) provided by the data contributor.
orgDpth	integer	Organic layer thickness measured from the ground/moss surface to the organic-mineral interface, as a site mean in cm, provided by the data contributor.
srfH2O	character	A categorical variable describing if plot locations experience seasonal inundation (i.e., standing surface water during the early season but dry by late season). Seasonal inundation (Y: yes) or not (N: no) or unknown (U). Provided by the data contributor.
msrType	character	A categorical variable of thaw (T) or active (A). Active refers to active layer thickness (i.e., maximum seasonal thaw at the end of growing season), and thaw refers to thaw depth (i.e., less than seasonal maximum taken earlier than the end of thawing season). Provided by the data contributor.
msrDoy	integer	Day of year (DOY) for the day of measurement converted from YYYY-MM-DD.
msrDepth	float	The field measurement of the thaw depth or ALT in cm. Provided by the data contributor.
topoPos	character	Categorical variable describing the topographic position of plot locations as upland (U), midslope (M), lowland (L). Provided by the data contributor.
slope	integer	Numeric value indicating slope angle provided by the data contributor.
vegCvr	character	Evergreen needle-leaf (EN); broadleaf deciduous (BD); deciduous needle-leaf (DN); mixed needle-leaf majority MNM; mixed (M); mixed broadleaf majority (MBM); barrens (B), graminoid tussock dominated (GT), graminoid non-tussock dominated (GNT), prostrate shrub dominated (P), erect-shrub dominated (S), and wetlands (W). Provided by the data contributor.
resBiome	character	Biome assigned by spatial join with the Resolve data product 'BIOME_NAME' (Dinerstein et al., 2017).
resName	character	Ecozone name assigned by spatial join with the Resolve data product 'ECO_NAME' (Dinerstein et al., 2017).
permaExtent	character	Permafrost extent assigned by spatial join with permafrost ground-ice map 'EXTENT' as C=continuous, D=discontinuous, S=sporadic (Brown et al., 1998).
estDoy	integer	The day of year used to estimate ALT based on when the five-day mean daily air temperature shifted from above- to below-freezing.
estDepth	float	The estimated ALT in cm; calculated using air temperature from ERA5-Land and field measured thaw depth.
paired	character	Identifying code to pair unburned measurements to burned measurements provided by the data contributor.
tsf	integer	Time since fire calculated by subtracting year from fireYr.
tsfClass	character	Binned time since fire (tsf) classes in years as "unburned", "0-3", "4-10", "11-20", "21-40", ">40"

273

274



275 **2.6 Aggregating to compare burned to unburned measurements**

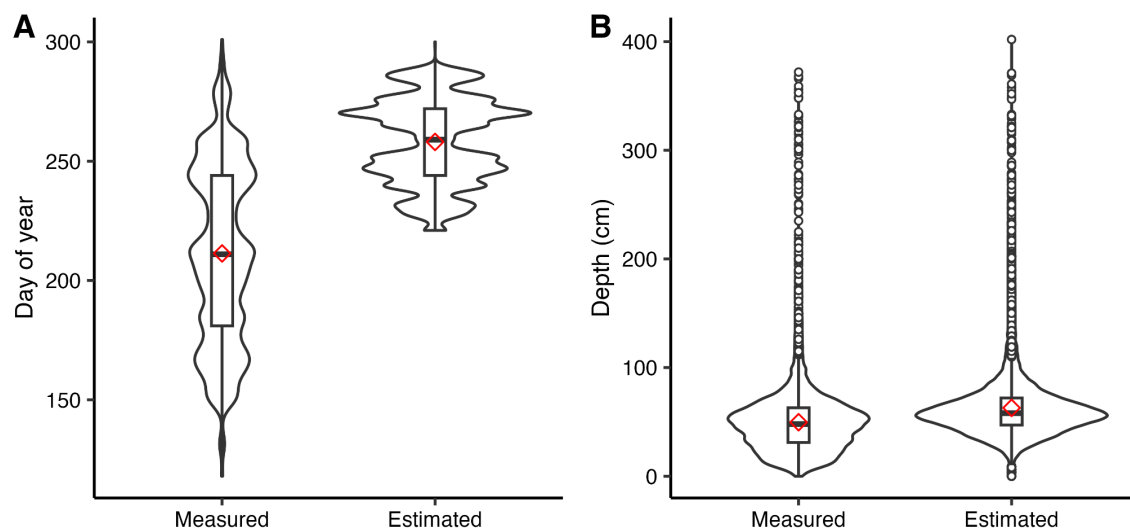
276 Paired burned and unburned sites are a unique and defining characteristic of this dataset. Data contributors were required to
277 provide details on how their burned measurements paired with unburned measurements. Site characteristics of unburned sites
278 were required to be representative of biogeoclimatic conditions prefire and within close proximity to their paired burned site(s).
279 The dataset includes a code to link burned with unburned sites ('paired'). To examine the difference between burned and
280 unburned sites, measurements were aggregated by ecozone ('resName'), data contributor ('submitNm'), burned or unburned
281 ('distur'), pairing code ('paired'), year of the fire event ('fireYr'), and can be further grouped by time since fire ('tsf') (Table
282 4).

283 **3 Data summary**

284 **3.1 General Characteristics of the data**

285 In total, the final dataset includes 47,952 observations from the original 52,466 observations. Thaw depth measurements are
286 predominantly from North America, with 35,794 (19,338 burned, 15,434 unburned) in Alaska and 12,587 (7,528 burned, 4,276
287 unburned) in Canada, and 1,376 (8981 burned, 495 unburned) in Russia. These *in situ* measurements were collected within the
288 continuous, discontinuous, and sporadic permafrost zones (Fig. 1). Data were contributed with both burned and unburned
289 paired sites with fire years ranging from 1900 to 2022 across 112 fire events. There are 193 unique paired burned/unburned
290 measures based on pair id (76), fire year (37 unique years), fire events (63 unique events), and time since fire spread across 12
291 ecozones. There are 22,500 estimated observations across the boreal forests/taiga and 27,257 estimated observations across
292 the tundra biomes (Fig. 4). There are 27,201 observations from continuous permafrost, 13,798 from discontinuous permafrost,
293 and 8,758 from sporadic permafrost.

294



295

296 **Figure 5.** The distribution for *in situ* measurements vs. estimated measurements. For day of year (A) and thaw depth (B), we show
 297 the distribution for *in situ* measurements vs. estimated measurements using violin plots overlain with boxplots with a red diamond
 298 marking the mean. Measured day of year and depths were provided in the raw data contribution. The day of year shows a wide
 299 spread of dates, which is caused by the broad geographic extent of the data. Estimated values were calculated to create a dataset
 300 that characterises maximum thaw depth (i.e., ALT).

301

302 3.2 Estimated ALT

303 The estimated ALT provides a temporally consistent measurement capable of quantifying the effects of wildfire on active layer
 304 dynamics temporally and spatially. The data show the shift from measured thaw depth to estimated ALT characterised by a
 305 narrower range of dates and depth measurements (Fig. 5A & 5B). The day of year is condensed for the estimated measures
 306 (Fig. 5A), which was anticipated since the contributed data were collected throughout the thawing season resulting in a wide
 307 spread due to the broad geographic extent of the data whereas the estimated data were truncated to the later part of the thaw
 308 season, resulting in a narrow range of days. The uncertainty in the estimated ALT varies with biome and disturbance (Table 5,
 309 Fig. 6). Boreal burned values tend to underestimate by about five percent, whereas unburned values tend to overestimate by
 310 about 15 percent. For the tundra, burned and unburned values tend to be overestimated by 19.6 and 22.8 percent respectively.
 311 The sample size is much smaller for the tundra biome for estimating uncertainty.

312

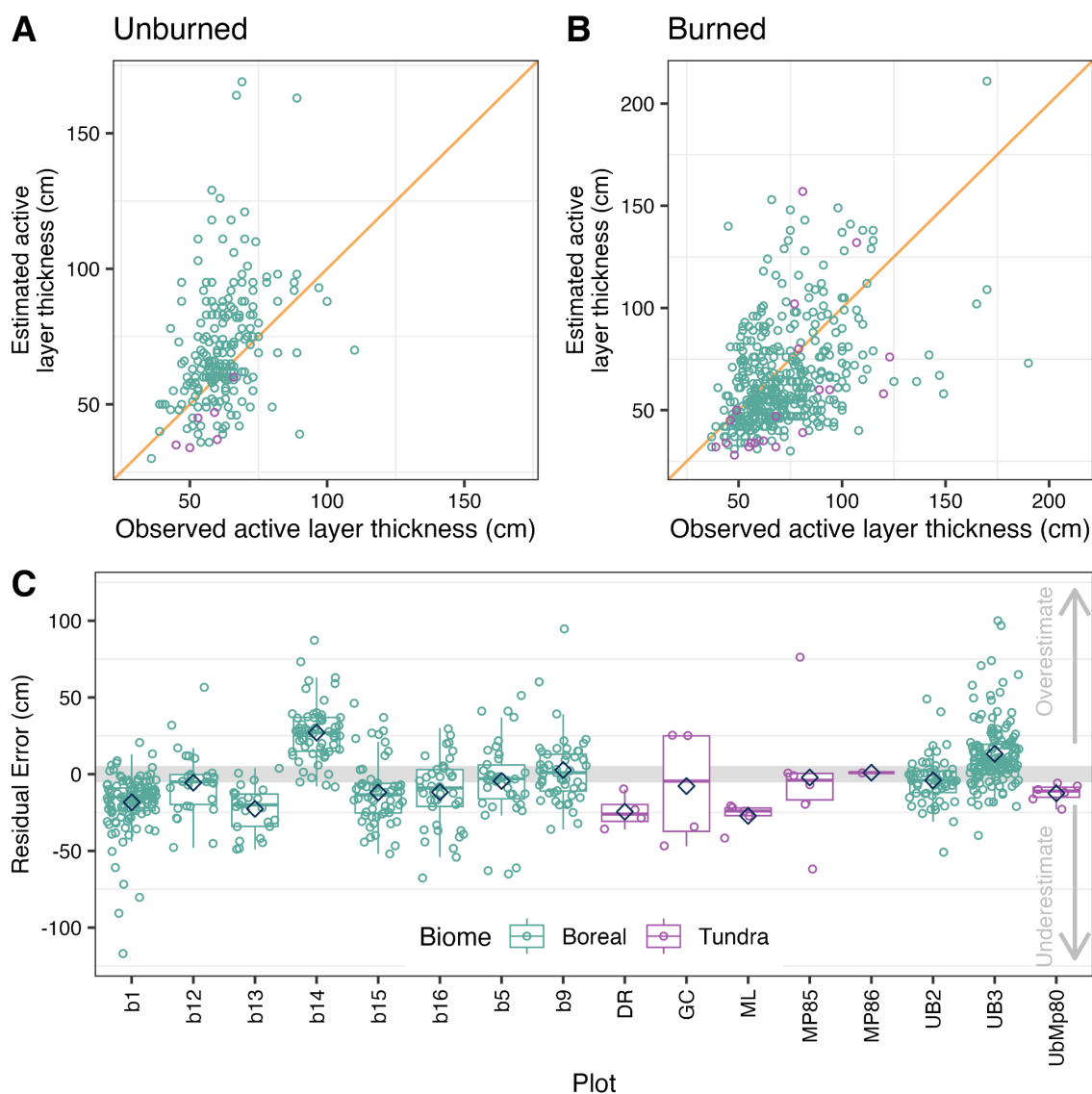
313 **Table 5.** Quantifying uncertainty for estimated ALT. We report the root mean square error (RMSE), percent uncertainty, mean
 314 residual error as an indication of bias, and sample size for burned and unburned sites in the validation dataset. Negative values
 315 indicate an overestimation and positive values indicate an underestimation.

Biome	Disturbance	RMSE	Percent uncertainty	Mean residual error (bias)	Sample size
Boreal	Burned	22.8	4.6	5.7	413



Boreal	Unburned	20.3	14.5	-8.4	212
Tundra	Burned	29.2	19.6	13.9	20
Tundra	Unburned	5.6	22.8	12.5	6

316



317

318 **Figure 6. Quantifying uncertainty of ALT estimates. Panel (A) and (B) show observed depths compared to estimated depths split by**
 319 **unburned and burned sites with the orange line showing a slope of one. Panel (C) shows the bias by plot identifier, where zero**
 320 **indicates no difference between the observed and estimated values. Negative values indicate an underestimation and positive values**
 321 **indicate an overestimation with the mean shown by the blue diamond. Unburned plots are ub2, ub3, and UbMp80.**

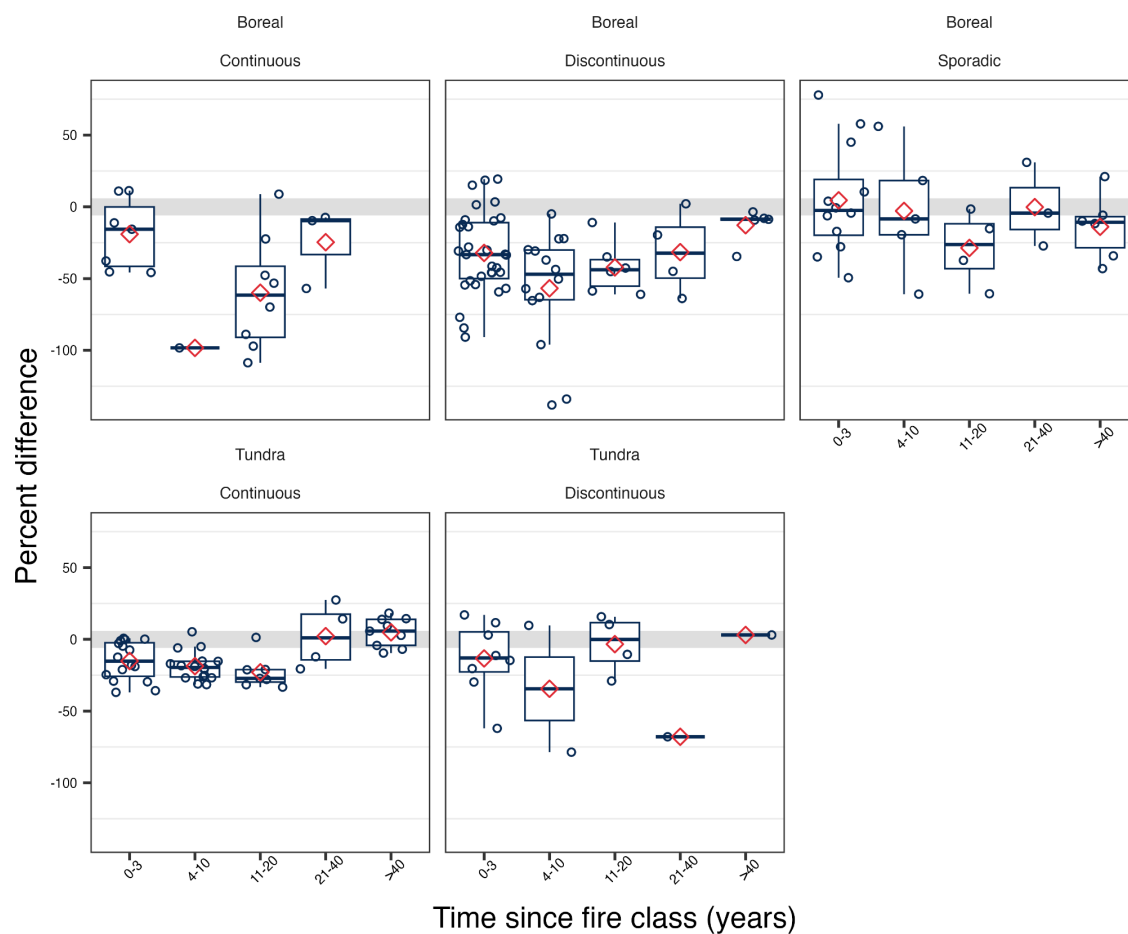


322

323 **3.3 Difference in estimated ALT between burned and unburned sites**

324 By aggregating the burned and unburned pairings, we show the percent difference in estimated ALT between burned and
325 unburned sites post-fire (Fig. 7, S3, S4). Most sites show a thickening of the active layer post-fire compared to adjacent
326 unburned sites. Generally, across boreal sites the mean percent difference shows a thickening of the active layer in the two
327 decades following fire, followed by a recovery in the subsequent decades (e.g., time since fire 21-40 and >40). The magnitude
328 of difference varies by biome and permafrost extent. In the boreal forest continuous permafrost region, the means follow this
329 general trend of expansion followed by recovery, however, there is very limited and no data at 4-10 years and >40 years,
330 respectively. The boreal forest discontinuous permafrost region follows the general trend, whereas the boreal forest sporadic
331 permafrost region shows a lower percent difference in the two decades following fire where the active layer does expand but
332 not to the same extent as seen in the continuous or discontinuous permafrost following a varied recovery at 21-40 and >40
333 years. The tundra biome follows the same general trend that the boreal sites do where mean percent difference shows a
334 thickening of the active layer in the two decades following fire, followed by a recovery in the subsequent decades (e.g., time
335 since fire 21-40 and >40). This trend is most distinct for tundra sites with continuous permafrost, whereas sites with
336 discontinuous permafrost show a bit more variability for 11-20, 21-40, and >40 years. The tundra sites with discontinuous
337 permafrost have a sample of one for 21-40 and >40 years, which makes it challenging to fully understand the recovery trend.
338 The trend of post-fire thickening of the active layer followed by recovery illustrates the effect of climate on permafrost
339 recovery. The variability in the extent of the thickening of the active layer across permafrost zones might provide insight to
340 potential future patterns. Specifically, the reduced thickening seen in the warmer boreal sporadic region might be a future
341 pattern that we see extending to the boreal discontinuous zone as the climate continues to warm.

342



343

344 **Figure 7.** Percent difference in estimated ALT between burned and unburned paired sites in the years following wildfire. The percent
345 difference is calculated $(\text{unburned} - \text{burned}) / ((\text{unburned} + \text{burned}) / 2) * 100$. Negative values indicate that the burned sites have a
346 thicker active layer than the unburned site, while values around zero show little difference in ALT, and positive values indicate that
347 unburned sites have a thicker active layer than the burned ALT. The red diamond indicates the mean based on paired burned-
348 unburned and then aggregated by time since fire class, permafrost extent, and biome. The box and whisker plots show the split in
349 quantiles. See Supplemental Materials to see a similar plot by ecozone (Fig. S3 and S4).

350 4 Strengths, Limitations, and Opportunities

351 4.1 Strengths

352 The FireALT dataset (Talucci et al., 2024) offers paired burned and unburned sites that can be aggregated and viewed both
353 spatially and temporally to provide critical insights for understanding wildfire impacts on ALT, a feature commonly used to
354 determine permafrost conditions. Field data collection is often spatially and temporally opportunistic, making comparisons of
355 disparate datasets difficult. For example, several geographically similar sites had depth measurements collected across a wide



356 range of dates throughout August and September, but these measurements were not necessarily capturing the maximum ALT
357 and therefore not comparable. Further, it is challenging to compare early to end of season thaw depth measurements (Holloway
358 and Lewkowicz 2020). By estimating ALT, the data can be used to extrapolate beyond individual measurements and provide
359 broader understanding of spatial and temporal feedbacks between wildfires, permafrost, and climate. Additionally, data include
360 several environment attributes, e.g., organic layer depth, slope, topographic position, and whether surface water was present.
361 Future analyses could integrate these environmental variables to expound upon the relationship between environmental
362 variables, ALT, and wildfire. Finally, we show a general expansion of the active layer following fire followed by recovery 40
363 years post-fire but the magnitude of expansion and recovery vary by biome and permafrost zone, pointing to the role of
364 vegetation, permafrost conditions, and climate on active layer dynamics in response to wildfire (Brown et al., 2015). Climate
365 has changed over the time period of the fire events captured within this dataset. Generally, the data indicates that we may
366 expect the active layer to fully recover 40 years post-fire, but that may change for more recent fires. The boreal sporadic zone
367 experiences less expansion of the active layer with a less distinct recovery, which demonstrates how climate influences active
368 layer recovery in warmer regions. This illustrates how climate influences permafrost recovery, and with a warming climate,
369 we may expect to see patterns more like this in boreal discontinuous permafrost zone.

370

371 **4.2 Limitations**

372 Estimating ALT is crucial for spatial-temporal evaluations of wildfire-permafrost interactions due to the variability in thaw
373 depth throughout the thaw season. However, uncertainties arise in the estimated ALT from the data we integrate to make those
374 calculations. Air temperature can be a reliable metric for calculating maximum ALT (Osterkamp and Burn 2002, Holloway
375 and Lewkowicz 2020), but the coarse resolution climate data and *in situ* weather station gaps (Clelland et al. 2024), as well as
376 the lack of accounting for disturbance effects on air temperature (Kurylyk and Hayashi, 2016, Muñoz-Sabater et al., 2021,
377 Helbig et al., 2024), all impact the accuracy of the estimated ALT. The Stefan equation assumes negligible soil heat capacity
378 and thus can overestimate thaw depth, and it also does not account for fire altering the surface energy balance (e.g., reducing
379 albedo, loss of canopy and shading) and heat fluxes (e.g., loss of above-ground biomass), all of which increase thaw depths
380 and can contribute to underestimations of ALT (Kurylyk and Hayashi, 2016). Our quantification of uncertainty supports this
381 underestimation bias for burned sites and over estimation for unburned sites in the boreal biome. Further, the lack of inclusion
382 of frozen water content in the Stefan equation may affect early season measurements due to the zero curtain, where the rate of
383 thawing may not scale directly with air temperature (Osterkamp, 1987, Romanovsky and Osterkamp, 2000). These effects
384 likely vary between tundra and boreal sites. These are dynamic systems with multiple feedbacks that influence the freeze-thaw
385 cycle and the timing of maximum thaw depth. Interannual variability in ALT is dependent on temperature, precipitation, and
386 fluctuations in thaw season length, which are a source of uncertainty in our approach (Shur et al., 2005). Although there are
387 uncertainties, estimating ALT allows for valuable comparisons between sites that are not feasible with the raw data.

388



389 Burn severity is a critical component of wildfire that impacts ALT and permafrost stability through combustion of the
390 insulating organic matter, vegetation and post-fire changes in albedo (Rocha and Shaver 2011, Alexander et al., 2018). We do
391 not account for burn severity in the data, which could strongly influence differences we see between burned and unburned
392 ALT. Burn severity could be estimated using the organic depth measurement in the data, but the organic depth will be
393 influenced by time since fire or through the integration of satellite imagery that could be used as a proxy for burn severity.
394 However, vegetation indices that estimate burn severity (e.g., differenced Normalized Burn Ratio [dNBR]) are typically better
395 correlated with aboveground burn severity while less indicative of burn depth (e.g., Delcourt et al., 2021). Recent research
396 which has shown combinations of remote sensing proxies, dNBR, and land surface temperature could be used in conjunction
397 with these field measurements to estimate changes in ALT across fire scars (Diaz et al., 2024). Additionally, the ice content of
398 permafrost may impact the interaction between wildfire and permafrost, with direct effects on ALT particularly where
399 subsidence is involved or where the increase in ALT contributes to the degradation of ice-rich permafrost (e.g., Yedoma) in
400 the short-term (Nelson et al., 2021, Strauss et al., 2021, Jones et al., 2024).

401 **4.3 Representativeness of the data**

402 The data included in our dataset are predominantly from North America, and there are large spatial gaps across the northern
403 high latitude permafrost region (Fig. S5). For example, Russia is underrepresented despite containing 65% of the northern
404 high-latitude permafrost (Anisimov and Reneva 2006, Streletskiy et al., 2019) and a majority of the burned area within the
405 northern permafrost region (Lorantý et al., 2016). The lack of data for this region is further exacerbated by the Russian invasion
406 of Ukraine (López-Blanco et al., 2024), which has impacted international collaborations. Additionally, some of the spatial
407 gaps could be a function of the submission criteria that required a burned/unburned pair. Due to the remoteness of northern
408 high latitude fires, field campaigns may be constrained spatially and temporally based on accessibility of field sites and timing
409 of field campaigns. Opportunistic site selection introduces bias into the dataset; however, this is unavoidable for the data
410 synthesis effort that relies on contributions of existing data.

411 **4.4 Future research opportunities**

412 There is opportunity to expand this dataset to increase the spatio-temporal coverage of the data to better understand impacts
413 of wildfire on permafrost dynamics. While we touch on how ALT differs across burned and unburned sites across the northern
414 high latitude permafrost zone, further investigation is warranted on the role of wildfire on permafrost dynamics. We have
415 identified several understudied research areas that could be augmented with this dataset. First, the dataset could be used to
416 further investigate the geospatial distribution of permafrost recovery following fire across the northern high latitude permafrost
417 zone. Second, these data could be used to determine the probability (i.e., likelihood) of permafrost recovery after wildfire as a
418 function of ecotype or ecoclimatic zone, permafrost classification, fire rotation period, and/or climate. Third, the data could
419 aid in determining the soil C consequences of temporary or permanent post-fire permafrost degradation. Fourth, investigations
420 could be structured to identify changes in wildfire activity that affects the likelihood of permafrost recovery/degradation and



421 associated soil C vulnerability using predictive mapping. Fifth, the data could be used to develop an organic layer deficit value
422 that would represent the difference between the organic layer thickness in the burn scar with the organic layer thickness in the
423 unburned control site. Sixth, this dataset could be augmented with quantification of subsidence and the combination of that
424 with ALT to understand how much new permafrost is exposed to seasonal thaw as a result of fire. Finally, there is the
425 opportunity for this dataset to be used in algorithm development, calibration, and validation for evolving process-based models
426 that are trying to capture the impact of fires on permafrost.

427 **5 Data use guidelines & availability**

428 The FireALT dataset (Talucci et al., 2024) are publicly available for download through the Arctic Data Center under a Creative
429 Commons Attribution 4.0 International copyright (CC BY 4.0). Data should be appropriately referenced by citing this paper
430 and the dataset (see Arctic Data Center). Users of the data are invited to ask questions by contacting the dataset developers.
431 We recommend that researchers planning to use this data as a core portion of their analysis collaborate with the data developers
432 and relevant individual site contributors. The data are available for download as a csv file through the Arctic Data Center
433 (<https://doi.org/10.18739/A2W950Q33>).
434

435 **6 Conclusions**

436 The FireALT dataset offers a collection of paired burned and unburned sites with measured thaw depths and estimated ALT.
437 By estimating ALT, we address a key challenge: the ability to assess impacts of wildfire on ALT when measurements are
438 taken at various times throughout the thaw season depending on the time of field campaigns (typically June through August).
439 This dataset can be utilised for future research activities that can expand understanding of the feedbacks between permafrost,
440 wildfire, and global climate systems. Changes to the active layer serve as an important diagnostic indicator that requires
441 continuous monitoring under the current dynamic climate conditions to further understand temporary or permanent changes to
442 permafrost and subsequent losses in carbon storage. These types of data synthesis efforts are crucial for addressing
443 understudied research areas particularly algorithm development, calibration, and validation for evolving process-based models
444 as well as extrapolating across space and time, which will elucidate permafrost-wildfire interactions under accelerated warming
445 across the high northern latitude permafrost zone.

446 **Author contributions**

447 The FireALT dataset was conceptualised during the 2019 Permafrost Carbon Network meeting by ACT, BMR, DO, KLM,
448 LTB, MAW, MJL, MML with additional input by ACT, AKP, AVR, BMR, JAO, JEH, KLM, LTB, MAW, MJL, MRT, NB,



449 REH, SMN, SV for the methods. Data curation was carried out by AB, ACT, AKP, AS, AVR, BB, BVG, CJFD, CM, CMD,
450 DO, GVF, HDA, JAO, JEH, JLB, KLM, LB, LBS, LRD, LTB, MCM, MML, MRT, MTJ, NB, OS, RAL, REH, SMN, SS,
451 SV, TAD, TAS, TH. Formal analysis was performed by ACT, JEH, MML. ACT and MML provided project management.
452 BMR, MML provided supervision. Visualisations were created by ACT, JEH, JD. ACT, JEH, MML wrote the original draft.
453 All authors contributed to the realisation of the permafrost wildfire data and participated in the editing of the manuscript.
454

455 **Competing Interests**

456 S. Veraverbeke is a member of the editorial board of ESSD. The contact author declares that they and all other co-authors have
457 no competing interests.
458

459 **Acknowledgments**

460 A. C. Talucci acknowledges Christina Shintani and Greg Fiske at Woodwell Climate Research Center for their cartographic
461 feedback and funding support from the NSF Arctic System Science (award no. 2116864). J. E. Holloway acknowledges Antoni
462 Lewkowicz at the University of Ottawa for the support for field data collections. B.M. Rogers recognizes support from the
463 Gordon and Betty Moore Foundation (grant no. 8414), NSF Arctic System Science (award no. 2116864), and funding
464 catalysed by the Audacious Project (Permafrost Pathways). J. O'Donnell acknowledges Jennifer Harden and support from the
465 U.S. Geological Survey for field data collections. D. Olefeldt acknowledges Carolyn Gibson for her field work contributions
466 to the contributed data. L. T. Berner was supported by the NASA Arctic Boreal Vulnerability Experiment (80NSSC22K1244
467 & 80NSSC22K1247). S.M. Natali acknowledges John Wood and the Polaris Project team for field support, and funding from
468 NSF (1417700, 1915307, 1561437) and NASA (NNX15AT81A). T.A. Douglas acknowledges the U.S. Department of
469 Defense's Strategic Environmental Research and Development Program (Project RC18- 1170) and Environmental Science
470 and Technology Certification Program (Project RC22-D3-7408) as well as the U.S. Army Engineer Research and Development
471 Center Basic Research Portfolio through Program Element PE 0601102A/T14/ST1409. S. Sistla and N. Baillargeon
472 acknowledge support from NSF 2218742. J.L. Baltzer acknowledges funding through the Government of the Northwest
473 Territories' Cumulative Impacts Monitoring Program Project 170, Canada First Research Excellence Fund's Global Water
474 Futures program (project Northern Water Futures), Natural Sciences and Engineering Research Council's Discovery Grant
475 funding, and the Canada Research Chairs program. Data collection was conducted under Aurora Research Institute's Scientific
476 Research License numbers 16815, 16755, 16311, 16018, 15879, and 15609. C. J. F. Delcourt acknowledges funding from the
477 Dutch Research Council (NWO) through a Vidi grant (grant no. 016.Vidi.189.070) and from the European Research Council
478 (ERC) through a Consolidator grant under the European Union's Horizon 2020 research and innovation program (grant no.



479 101000987), both awarded to S. Veraverbeke. T. A. Shestakova acknowledges funding from the Beatriu de Pinòs Programme
480 of the Government of Catalonia (2020 BP 00126). K. Manies acknowledges the support of the U.S. Geological Survey Earth
481 Surface Dynamics Program. A.K. Paulson and H. D. Alexander acknowledge Seth Robinson, Eric Borth, Sarah Frankenberg,
482 Aaron Lewis, Brian Izbicki, Clark Thompson, Jill Young, Amanda Ruland, and Elena Forbath for assistance with field work
483 and Valetin Spektor, Nikita Zimov, Sergei Davydov, and Sergei Zimov for contributing extensive knowledge of the region
484 and logistics support. We also acknowledge NSF OPP-2100773. G. V. Frost acknowledges funding from the Western Alaska
485 Landscape Conservation Cooperative (WALCC) award F16AC01215, NASA Arctic Boreal Vulnerability Experiment contract
486 NNH16CP09C. B.V. Gaglioti acknowledges Park Williams for fieldwork, and NSF Award 2124824 and the Joint Fire Science
487 Program Project 20-2-01-13 for funding. Thanks to Benjamin Maglio and Dana Brown for their assistance in reviewing this
488 manuscript. Thanks to the Arctic Data Center team for their assistance with archiving the dataset. Any use of trade, firm, or
489 product names is for descriptive purposes only and does not imply endorsement by the U.S. Government.
490

491 **References**

- 492 Alexander, H. D., Natali, S. M., Loranty, M. M., Ludwig, S. M., Spektor, V. V., Davydov, S., Zimov, N., Trujillo, I., and
493 Mack, M. C.: Impacts of increased soil burn severity on larch forest regeneration on permafrost soils of far northeastern Siberia,
494 *Forest Ecology and Management*, 417, 144–153, <https://doi.org/10.1016/j.foreco.2018.03.008>, 2018.
495
- 496 Alexander, H. D., Paulson, A. K., DeMarco, J., Hewitt, R., Lichstein, J., Loranty, M. M., Mack, M. C., McEwan, R.,
497 Frankenberg, S., and Robinson, S.: Fire influences on forest recovery and associated climate feedbacks in Siberian Larch
498 Forests, Russia, 2018-2019, <https://doi.org/10.18739/A2XG9FB90>, 2020.
499
- 500 Amiro, B. D.: Paired-tower measurements of carbon and energy fluxes following disturbance in the boreal forest, *Global*
501 *Change Biology*, 7, 253–268, <https://doi.org/10.1046/j.1365-2486.2001.00398.x>, 2001.
502
- 503 Amiro, B. D., Orchansky, A. L., Barr, A. G., Black, T. A., Chambers, S. D., Chapin Iii, F. S., Goulden, M. L., Litvak, M., Liu,
504 H. P., McCaughey, J. H., McMillan, A., and Randerson, J. T.: The effect of post-fire stand age on the boreal forest energy
505 balance, *Agricultural and Forest Meteorology*, 140, 41–50, <https://doi.org/10.1016/j.agrformet.2006.02.014>, 2006.
506
- 507 Anisimov, O. and Reneva, S.: Permafrost and Changing Climate: The Russian Perspective, *AMBIO: A Journal of the Human*
508 *Environment*, 35, 169–175, [https://doi.org/10.1579/0044-7447\(2006\)35\[169:PACCTR\]2.0.CO;2](https://doi.org/10.1579/0044-7447(2006)35[169:PACCTR]2.0.CO;2), 2006.
509



- 510 Baillargeon, N., Pold, G., Natali, S. M., and Sistla, S. A.: Lowland tundra plant stoichiometry is somewhat resilient decades
511 following fire despite substantial and sustained shifts in community structure, *Arctic, Antarctic, and Alpine Research*, 54, 525–
512 536, <https://doi.org/10.1080/15230430.2022.2121246>, 2022.
- 513
- 514 Baltzer, J. L., Veness, T., Chasmer, L. E., Sniderhan, A. E., and Quinton, W. L.: Forests on thawing permafrost: fragmentation,
515 edge effects, and net forest loss, *Global Change Biology*, 20, 824–834, <https://doi.org/10.1111/gcb.12349>, 2014.
- 516
- 517 Bonnaventure, P. P. and Lamoureux, S. F.: The active layer: A conceptual review of monitoring, modeling techniques and
518 changes in a warming climate, *Progress in Physical Geography: Earth and Environment*, 37, 352–376,
519 <https://doi.org/10.1177/0309133313478314>, 2013.
- 520
- 521 Bret-Harte, M. S., Mack, M. C., Shaver, G. R., Huebner, D. C., Johnston, M., Mojica, C. A., Pizano, C., and Reiskind, J. A.:
522 The response of Arctic vegetation and soils following an unusually severe tundra fire, *Phil. Trans. R. Soc. B*, 368, 20120490,
523 <https://doi.org/10.1098/rstb.2012.0490>, 2013.
- 524
- 525 Brown, D. R. N., Jorgenson, M. T., Douglas, T. A., Romanovsky, V. E., Kielland, K., Hiemstra, C., Euskirchen, E. S., and
526 Ruess, R. W.: Interactive effects of wildfire and climate on permafrost degradation in Alaskan lowland forests, *JGR*
527 *Biogeosciences*, 120, 1619–1637, <https://doi.org/10.1002/2015JG003033>, 2015.
- 528
- 529 Brown, J., Ferrians, O., Heginbottom, J. A., and Melnikov, E.: Circum-Arctic Map of Permafrost and Ground-Ice Conditions,
530 Version 2 [Data Set], <https://doi.org/10.7265/skbg-kf16>, 1998.
- 531
- 532 Brown, J., Hinkel, K. M., and Nelson, F. E.: The circumpolar active layer monitoring (calm) program: Research designs and
533 initial results, *Polar Geography*, 24, 166–258, <https://doi.org/10.1080/10889370009377698>, 2000.
- 534
- 535 Byrne, B., Liu, J., Bowman, K. W., Pascolini-Campbell, M., Chatterjee, A., Pandey, S., Miyazaki, K., Van Der Werf, G. R.,
536 Wunch, D., Wennberg, P. O., Roehl, C. M., and Sinha, S.: Carbon emissions from the 2023 Canadian wildfires, *Nature*, 633,
537 835–839, <https://doi.org/10.1038/s41586-024-07878-z>, 2024.
- 538
- 539 Burn, C. R. and Lewkowicz, A. G.: Canadian Landform Examples - 17: Retrogressive thaw slumps, *Canadian Geographies /*
540 *Géographies canadiennes*, 34, 273–276, <https://doi.org/10.1111/j.1541-0064.1990.tb01092.x>, 1990.
- 541
- 542 Calvin, K., Dasgupta, D., Krinner, G., Mukherji, A., Thorne, P. W., Trisos, C., Romero, J., Aldunce, P., Barrett, K., Blanco,
543 G., Cheung, W. W. L., Connors, S., Denton, F., Diongue-Niang, A., Dodman, D., Garschagen, M., Geden, O., Hayward, B.,



- 544 Jones, C., Jotzo, F., Krug, T., Lasco, R., Lee, Y.-Y., Masson-Delmotte, V., Meinshausen, M., Mintenbeck, K., Mokssit, A.,
545 Otto, F. E. L., Pathak, M., Pirani, A., Poloczanska, E., Pörtner, H.-O., Revi, A., Roberts, D. C., Roy, J., Ruane, A. C., Skea, J.,
546 Shukla, P. R., Slade, R., Slangen, A., Sokona, Y., Sörensson, A. A., Tignor, M., Van Vuuren, D., Wei, Y.-M., Winkler, H.,
547 Zhai, P., Zommers, Z., Hourcade, J.-C., Johnson, F. X., Pachauri, S., Simpson, N. P., Singh, C., Thomas, A., Totin, E., Arias,
548 P., Bustamante, M., Elgizouli, I., Flato, G., Howden, M., Méndez-Vallejo, C., Pereira, J. J., Pichs-Madruga, R., Rose, S. K.,
549 Saheb, Y., Sánchez Rodríguez, R., Ürge-Vorsatz, D., Xiao, C., Yassaa, N., Alegría, A., Armour, K., Bednar-Friedl, B., Blok,
550 K., Cissé, G., Dentener, F., Eriksen, S., Fischer, E., Garner, G., Guivarch, C., Haasnoot, M., Hansen, G., Hauser, M., Hawkins,
551 E., Hermans, T., Kopp, R., Leprince-Ringuet, N., Lewis, J., Ley, D., Ludden, C., Niamir, L., Nicholls, Z., Some, S., Szopa, S.,
552 Trewin, B., Van Der Wijst, K.-I., Winter, G., Witting, M., Birt, A., Ha, M., et al.: IPCC, 2023: Climate Change 2023: Synthesis
553 Report. Contribution of Working Groups I, II and III to the Sixth Assessment Report of the Intergovernmental Panel on Climate
554 Change [Core Writing Team, H. Lee and J. Romero (eds.)]. IPCC, Geneva, Switzerland., Intergovernmental Panel on Climate
555 Change (IPCC), <https://doi.org/10.59327/IPCC/AR6-9789291691647>, 2023.
- 556
- 557 Chambers, S. D., Beringer, J., Randerson, J. T., and Chapin, F. S.: Fire effects on net radiation and energy partitioning:
558 Contrasting responses of tundra and boreal forest ecosystems, *J. Geophys. Res.*, 110, 2004JD005299,
559 <https://doi.org/10.1029/2004JD005299>, 2005.
- 560
- 561 Chambers, S. D. and Chapin, F. S.: Fire effects on surface-atmosphere energy exchange in Alaskan black spruce ecosystems:
562 Implications for feedbacks to regional climate, *J. Geophys. Res.*, 107, <https://doi.org/10.1029/2001JD000530>, 2002.
- 563
- 564 Clelland, A. A., Marshall, G. J., and Baxter, R.: Evaluating the performance of key ERA-INTERIM , ERA5 and ERA5-LAND
565 climate variables across Siberia, *Intl Journal of Climatology*, 44, 2318–2342, <https://doi.org/10.1002/joc.8456>, 2024.
- 566
- 567 Dearborn, K. D., Wallace, C. A., Patankar, R., and Baltzer, J. L.: Permafrost thaw in boreal peatlands is rapidly altering forest
568 community composition, *Journal of Ecology*, 109, 1452–1467, <https://doi.org/10.1111/1365-2745.13569>, 2021.
- 569
- 570 de Groot, W. J., Flannigan, M. D., and Cantin, A. S.: Climate change impacts on future boreal fire regimes, *Forest Ecology*
571 *and Management*, 294, 35–44, <https://doi.org/10.1016/j.foreco.2012.09.027>, 2013.
- 572
- 573 Delcourt, C. J. F., Combee, A., Izbicki, B., Mack, M. C., Maximov, T., Petrov, R., Rogers, B. M., Scholten, R. C., Shestakova,
574 T. A., Van Wees, D., and Veraverbeke, S.: Evaluating the Differenced Normalized Burn Ratio for Assessing Fire Severity
575 Using Sentinel-2 Imagery in Northeast Siberian Larch Forests, *Remote Sensing*, 13, 2311, <https://doi.org/10.3390/rs13122311>,
576 2021.
- 577



- 578 Delcourt, C. J. F., Rogers, B. M., Akhmetzyanov, L., Izbicki, B., Scholten, R. C., Shestakova, T., van Wees, D., Mack, M. C.,
579 Sass-Klaassen, U., and Veraverbeke, S.: Burned and Unburned Boreal Larch Forest Site Data, Northeast Siberia,
580 <https://doi.org/10.5281/zenodo.10840088>, 2024.
- 581
- 582 Derksen, C., Burgess, D., Duguay, C., Howell, S., Mudryk, L., Smith, S., Thackeray, C., and Kirchmeier-Young, M.: Changes
583 in snow, ice, and permafrost across Canada, in: Canada's Changing Climate Report, Government of Canada, Ottawa, Ontario,
584 194–260, 2019.
- 585
- 586 Descals, A., Gaveau, D. L. A., Verger, A., Sheil, D., Naito, D., and Peñuelas, J.: Unprecedented fire activity above the Arctic
587 Circle linked to rising temperatures, *Science*, 378, 532–537, <https://doi.org/10.1126/science.abn9768>, 2022.
- 588
- 589 Diaz, L. R., Delcourt, C. J. F., Langer, M., Loranty, M. M., Rogers, B. M., Scholten, R. C., Shestakova, T. A., Talucci, A. C.,
590 Vonk, J. E., Wangchuk, S., and Veraverbeke, S.: Environmental drivers and remote sensing proxies of post-fire thaw depth in
591 Eastern Siberian larch forests, <https://doi.org/10.5194/egusphere-2024-469>, 21 March 2024.
- 592
- 593 Dieleman, C.M., Day, N.J., Holloway, J.E., Baltzer, J., Douglas, T.A., Turetsky, M.R.. Carbon and nitrogen cycling dynamics
594 following permafrost thaw in the Northwest Territories, 845, 157288, <https://doi-org./10.1016/j.scitotenv.2022.157288>, 2022
- 595
- 596
- 597 Dinerstein, E., Olson, D., Joshi, A., Vynne, C., Burgess, N. D., Wikramanayake, E., Hahn, N., Palminteri, S., Hedao, P., Noss,
598 R., Hansen, M., Locke, H., Ellis, E. C., Jones, B., Barber, C. V., Hayes, R., Kormos, C., Martin, V., Crist, E., Sechrest, W.,
599 Price, L., Baillie, J. E. M., Weeden, D., Suckling, K., Davis, C., Sizer, N., Moore, R., Thau, D., Birch, T., Potapov, P.,
600 Turubanova, S., Tyukavina, A., De Souza, N., Pintea, L., Brito, J. C., Llewellyn, O. A., Miller, A. G., Patzelt, A., Ghazanfar,
601 S. A., Timberlake, J., Klöser, H., Shennan-Farpón, Y., Kindt, R., Lillesø, J.-P. B., Van Breugel, P., Graudal, L., Voge, M., Al-
602 Shammari, K. F., and Saleem, M.: An Ecoregion-Based Approach to Protecting Half the Terrestrial Realm, *BioScience*, 67,
603 534–545, <https://doi.org/10.1093/biosci/bix014>, 2017.
- 604
- 605 Douglas, T. A., Jorgenson, M. T., Brown, D. R. N., Campbell, S. W., Hiemstra, C. A., Saari, S. P., Bjella, K., and Liljedahl,
606 A. K.: Degrading permafrost mapped with electrical resistivity tomography, airborne imagery and LiDAR, and seasonal thaw
607 measurements, *GEOPHYSICS*, 81, WA71–WA85, <https://doi.org/10.1190/geo2015-0149.1>, 2016.
- 608
- 609 Douglas, T. A., Turetsky, M. R., and Koven, C. D.: Increased rainfall stimulates permafrost thaw across a variety of Interior
610 Alaskan boreal ecosystems, *npj Clim Atmos Sci*, 3, 28, <https://doi.org/10.1038/s41612-020-0130-4>, 2020.
- 611



- 612 Fisher, J. P., Estop-Aragonés, C., Thierry, A., Charman, D. J., Wolfe, S. A., Hartley, I. P., Murton, J. B., Williams, M., and
613 Phoenix, G. K.: The influence of vegetation and soil characteristics on active-layer thickness of permafrost soils in boreal
614 forest, *Glob Change Biol*, 22, 3127–3140, <https://doi.org/10.1111/gcb.13248>, 2016.
- 615
- 616 Fraser, R., Kokelj, S., Lantz, T., McFarlane-Winchester, M., Olthof, I., and Lacelle, D.: Climate Sensitivity of High Arctic
617 Permafrost Terrain Demonstrated by Widespread Ice-Wedge Thermokarst on Banks Island, *Remote Sensing*, 10, 954,
618 <https://doi.org/10.3390/rs10060954>, 2018.
- 619
- 620 Freitag, D. and McFadden, T.: *Introduction to Cold Regions Engineering*, 166–169, 1997.
- 621
- 622 Frost, G. V., Loehman, R. A., Nelson, P. R., and Paradis, D. P.: ABoVE: Vegetation Composition across Fire History Gradients
623 on the Y-K Delta, Alaska, <https://doi.org/10.3334/ORNLDAAC/1772>, 2020.
- 624
- 625 Gaglioti, B. V., Berner, L. T., Jones, B. M., Orndahl, K. M., Williams, A. P., Andreu-Hayles, L., D’Arrigo, R. D., Goetz, S.
626 J., and Mann, D. H.: Tussocks Enduring or Shrubs Greening: Alternate Responses to Changing Fire Regimes in the Noatak
627 River Valley, Alaska, *J Geophys Res Biogeosci*, 126, <https://doi.org/10.1029/2020JG006009>, 2021.
- 628
- 629 Gasser, T., Kechiar, M., Ciais, P., Burke, E. J., Kleinen, T., Zhu, D., Huang, Y., Ekici, A., and Obersteiner, M.: Path-dependent
630 reductions in CO₂ emission budgets caused by permafrost carbon release, *Nature Geosci*, 11, 830–835,
631 <https://doi.org/10.1038/s41561-018-0227-0>, 2018.
- 632
- 633 Gibson, C. M., Brinkman, T., Cold, H., Brown, D., and Turetsky, M.: Identifying increasing risks of hazards for northern land-
634 users caused by permafrost thaw: integrating scientific and community-based research approaches, *Environ. Res. Lett.*, 16,
635 064047, <https://doi.org/10.1088/1748-9326/abfc79>, 2021.
- 636
- 637 Gibson, C. M., Chasmer, L. E., Thompson, D. K., Quinton, W. L., Flannigan, M. D., and Olefeldt, D.: Wildfire as a major
638 driver of recent permafrost thaw in boreal peatlands, *Nat Commun*, 9, 3041, <https://doi.org/10.1038/s41467-018-05457-1>,
639 2018.
- 640
- 641 Gorelick, N., Hancher, M., Dixon, M., Ilyushchenko, S., Thau, D., and Moore, R.: Google Earth Engine: Planetary-scale
642 geospatial analysis for everyone, *Remote Sensing of Environment*, 202, 18–27, <https://doi.org/10.1016/j.rse.2017.06.031>,
643 2017.
- 644



- 645 Hanes, C. C., Wang, X., Jain, P., Parisien, M.-A., Little, J. M., and Flannigan, M. D.: Fire-regime changes in Canada over the
646 last half century, *Can. J. For. Res.*, 49, 256–269, <https://doi.org/10.1139/cjfr-2018-0293>, 2019.
- 647
- 648 Harden, J. W., Manies, K. L., Turetsky, M. R., and Neff, J. C.: Effects of wildfire and permafrost on soil organic matter and
649 soil climate in interior Alaska: EFFECTS OF WILDFIRE AND PERMAFROST ON SOIL, *Global Change Biology*, 12, 2391–
650 2403, <https://doi.org/10.1111/j.1365-2486.2006.01255.x>, 2006.
- 651
- 652 Harris, S. A. and Permafrost Subcommittee, Associate Committee on Geotechnical Research, National Research Council of
653 Canada (Eds.): Glossary of permafrost and related ground-ice terms, Ottawa, Ontario, Canada, 156 pp., 1988.
- 654
- 655 Hayes, K. and Buma, B.: Effects of short-interval disturbances continue to accumulate, overwhelming variability in local
656 resilience, *Ecosphere*, 12, e03379, <https://doi.org/10.1002/ecs2.3379>, 2021.
- 657
- 658 Helbig, M., Daw, L., Iwata, H., Rudaitis, L., Ueyama, M., and Živković, T.: Boreal Forest Fire Causes Daytime Surface
659 Warming During Summer to Exceed Surface Cooling During Winter in North America, *AGU Advances*, 5, e2024AV001327,
660 <https://doi.org/10.1029/2024AV001327>, 2024.
- 661
- 662 Hollingsworth, T. N., Breen, A. L., Hewitt, R. E., and Mack, M. C.: Does fire always accelerate shrub expansion in Arctic
663 tundra? Examining a novel grass-dominated successional trajectory on the Seward Peninsula, Arctic, Antarctic, and Alpine
664 Research, 53, 93–109, <https://doi.org/10.1080/15230430.2021.1899562>, 2021.
- 665
- 666 Hollingsworth, T. N., Breen, A., Mack, M. C., and Hewitt, R. E.: Seward Peninsula post-fire vegetation and soil data from
667 multiple burns occurring from 1971 to 2012: “SPANFire” Study Sites, 2020.
- 668
- 669 Holloway, J.: Impacts of forest fire on permafrost in the discontinuous zones of northwestern Canada, University of Ottawa,
670 Ottawa, Ontario, 2020.
- 671
- 672 Holloway, J. E. and Lewkowicz, A. G.: Half a century of discontinuous permafrost persistence and degradation in western
673 Canada, *Permafrost and Periglac Process*, 31, 85–96, <https://doi.org/10.1002/ppp.2017>, 2020.
- 674
- 675 Holloway, J. E., Lewkowicz, A. G., Douglas, T. A., Li, X., Turetsky, M. R., Baltzer, J. L., and Jin, H.: Impact of wildfire on
676 permafrost landscapes: A review of recent advances and future prospects, *Permafrost and Periglac Process*, 31, 371–382,
677 <https://doi.org/10.1002/ppp.2048>, 2020.
- 678



- 679 Huang, B., Lu, F., Wang, X., Zheng, H., Wu, X., Zhang, L., Yuan, Y., and Ouyang, Z.: Ecological restoration is crucial in
680 mitigating carbon loss caused by permafrost thawing on the Qinghai-Tibet Plateau, *Commun Earth Environ*, 5, 341,
681 <https://doi.org/10.1038/s43247-024-01511-7>, 2024.
- 682
- 683 Hugelius, G., Strauss, J., Zubrzycki, S., Harden, J. W., Schuur, E. A. G., Ping, C.-L., Schirrmeister, L., Grosse, G., Michaelson,
684 G. J., Koven, C. D., O'Donnell, J. A., Elberling, B., Mishra, U., Camill, P., Yu, Z., Palmtag, J., and Kuhry, P.: Estimated stocks
685 of circumpolar permafrost carbon with quantified uncertainty ranges and identified data gaps, *Biogeosciences*, 11, 6573–6593,
686 <https://doi.org/10.5194/bg-11-6573-2014>, 2014.
- 687
- 688 Jafarov, E. E., Romanovsky, V. E., Genet, H., McGuire, A. D., and Marchenko, S. S.: The effects of fire on the thermal stability
689 of permafrost in lowland and upland black spruce forests of interior Alaska in a changing climate, *Environ. Res. Lett.*, 8,
690 035030, <https://doi.org/10.1088/1748-9326/8/3/035030>, 2013.
- 691
- 692 Jiang, Y., Rocha, A. V., O'Donnell, J. A., Drysdale, J. A., Rastetter, E. B., Shaver, G. R., and Zhuang, Q.: Contrasting soil
693 thermal responses to fire in Alaskan tundra and boreal forest: Contrasting soil thermal responses, *J. Geophys. Res. Earth Surf.*,
694 120, 363–378, <https://doi.org/10.1002/2014JF003180>, 2015.
- 695
- 696 Jones, B. M., Grosse, G., Arp, C. D., Miller, E., Liu, L., Hayes, D. J., and Larsen, C. F.: Recent Arctic tundra fire initiates
697 widespread thermokarst development, *Sci Rep*, 5, 15865, <https://doi.org/10.1038/srep15865>, 2015.
- 698
- 699 Jones, B. M., Kanevskiy, M. Z., Shur, Y., Gaglioti, B. V., Jorgenson, M. T., Ward Jones, M. K., Veremeeva, A., Miller, E. A.,
700 and Jandt, R.: Post-fire stabilization of thaw-affected permafrost terrain in northern Alaska, *Sci Rep*, 14, 8499,
701 <https://doi.org/10.1038/s41598-024-58998-5>, 2024.
- 702
- 703 Kasischke, E. S., Verbyla, D. L., Rupp, T. S., McGuire, A. D., Murphy, K. A., Jandt, R., Barnes, J. L., Hoy, E. E., Duffy, P.
704 A., Calef, M., and Turetsky, M. R.: Alaska's changing fire regime — implications for the vulnerability of its boreal forests
705 This article is one of a selection of papers from *The Dynamics of Change in Alaska's Boreal Forests: Resilience and Vulnerability*
706 in Response to Climate Warming., *Can. J. For. Res.*, 40, 1313–1324, <https://doi.org/10.1139/X10-098>, 2010.
- 707
- 708 Knoblauch, C., Beer, C., Liebner, S., Grigoriev, M. N., and Pfeiffer, E.-M.: Methane production as key to the greenhouse gas
709 budget of thawing permafrost, *Nature Clim Change*, 8, 309–312, <https://doi.org/10.1038/s41558-018-0095-z>, 2018.
- 710
- 711 Kurylyk, B. L. and Hayashi, M.: Improved Stefan Equation Correction Factors to Accommodate Sensible Heat Storage during
712 Soil Freezing or Thawing, *Permafrost & Periglacial*, 27, 189–203, <https://doi.org/10.1002/ppp.1865>, 2016.
- 713



- 714 Lewkowicz, A. G.: Dynamics of active-layer detachment failures, Fosheim Peninsula, Ellesmere Island, Nunavut, Canada,
715 Permafrost & Periglacial, 18, 89–103, <https://doi.org/10.1002/ppp.578>, 2007.
- 716
- 717 Li, X., Jin, H., He, R., Huang, Y., Wang, H., Luo, D., Jin, X., Lü, L., Wang, L., Li, W., Wei, C., Chang, X., Yang, S., and Yu,
718 S.: Effects of forest fires on the permafrost environment in the northern Da Xing'anling (Hinggan) mountains, Northeast China,
719 Permafrost & Periglacial, 30, 163–177, <https://doi.org/10.1002/ppp.2001>, 2019.
- 720
- 721 Liljedahl, A. K., Boike, J., Daanen, R. P., Fedorov, A. N., Frost, G. V., Grosse, G., Hinzman, L. D., Iijma, Y., Jorgenson, J.
722 C., Matveyeva, N., Necsoiu, M., Reynolds, M. K., Romanovsky, V. E., Schulla, J., Tape, K. D., Walker, D. A., Wilson, C. J.,
723 Yabuki, H., and Zona, D.: Pan-Arctic ice-wedge degradation in warming permafrost and its influence on tundra hydrology,
724 Nature Geosci, 9, 312–318, <https://doi.org/10.1038/ngeo2674>, 2016.
- 725
- 726 Liu, H., Randerson, J. T., Lindfors, J., and Chapin, F. S.: Changes in the surface energy budget after fire in boreal ecosystems
727 of interior Alaska: An annual perspective, J. Geophys. Res., 110, 2004JD005158, <https://doi.org/10.1029/2004JD005158>,
728 2005.
- 729
- 730 López-Blanco, E., Topp-Jørgensen, E., Christensen, T. R., Rasch, M., Skov, H., Arndal, M. F., Bret-Harte, M. S., Callaghan,
731 T. V., and Schmidt, N. M.: Towards an increasingly biased view on Arctic change, Nat. Clim. Chang., 14, 152–155,
732 <https://doi.org/10.1038/s41558-023-01903-1>, 2024.
- 733
- 734 Loranty, M. M., Lieberman-Cribbin, W., Berner, L. T., Natali, S. M., Goetz, S. J., Alexander, H. D., and Kholodov, A. L.:
735 Spatial variation in vegetation productivity trends, fire disturbance, and soil carbon across arctic-boreal permafrost ecosystems,
736 Environ. Res. Lett., 11, 095008, <https://doi.org/10.1088/1748-9326/11/9/095008>, 2016.
- 737
- 738 Mamet, S. D., Chun, K. P., Kershaw, G. G. L., Loranty, M. M., and Peter Kershaw, G.: Recent Increases in Permafrost Thaw
739 Rates and Areal Loss of Palsas in the Western Northwest Territories, Canada, Permafrost & Periglacial, 28, 619–633,
740 <https://doi.org/10.1002/ppp.1951>, 2017.
- 741
- 742 McCarty, J. L., Aalto, J., Paunu, V.-V., Arnold, S. R., Eckhardt, S., Klimont, Z., Fain, J. J., Evangeliou, N., Venäläinen, A.,
743 Tchebakova, N. M., Parfenova, E. I., Kupiainen, K., Soja, A. J., Huang, L., and Wilson, S.: Reviews and syntheses: Arctic fire
744 regimes and emissions in the 21st century, Biogeosciences, 18, 5053–5083, <https://doi.org/10.5194/bg-18-5053-2021>, 2021.
- 745
- 746 Muñoz Sabater, J.: ERA5-Land Daily Aggregated- ECMWF Climate Reanalysis, <https://doi.org/10.24381/cds.68d2bb30>,
747 2019.



- 748
- 749 Muñoz-Sabater, J., Dutra, E., Agustí-Panareda, A., Albergel, C., Arduini, G., Balsamo, G., Boussetta, S., Choulga, M.,
750 Harrigan, S., Hersbach, H., Martens, B., Miralles, D. G., Piles, M., Rodríguez-Fernández, N. J., Zsoter, E., Buontempo, C.,
751 and Thépaut, J.-N.: ERA5-Land: a state-of-the-art global reanalysis dataset for land applications, *Earth Syst. Sci. Data*, 13,
752 4349–4383, <https://doi.org/10.5194/essd-13-4349-2021>, 2021.
- 753
- 754 Natali, S.: Yukon-Kuskokwim Delta fire: thaw depth, soil temperature, and point-intercept vegetation, Yukon-Kuskokwim
755 Delta Alaska, 2015-2019., <https://doi.org/10.18739/A2707WP16>, 2018.
- 756
- 757 Natali, S., Kholodov, A. L., and Loranty, M. M.: Thaw depth and organic layer depth from Alaska borehole sites, 2015, 2017,
758 2018 (ViPER Project), <https://doi.org/10.18739/A22J6848J>, 2016.
- 759
- 760 Natali, S., Ludwig, S., Minions, C., and Watts, J. D.: ABoVE: Thaw Depth at Selected Unburned and Burned Sites Across
761 Alaska, 2016-2017., <https://doi.org/0.3334/ORNLDAAAC/1579..> 2018, 2018.
- 762
- 763 Natali, S. M., Holdren, J. P., Rogers, B. M., Treharne, R., Duffy, P. B., Pomerance, R., and MacDonald, E.: Permafrost carbon
764 feedbacks threaten global climate goals, *Proc. Natl. Acad. Sci. U.S.A.*, 118, e2100163118,
765 <https://doi.org/10.1073/pnas.2100163118>, 2021.
- 766
- 767 Nelson, F. E., Shiklomanov, N. I., and Nyland, K. E.: Cool, CALM, collected: the Circumpolar Active Layer Monitoring
768 program and network, *Polar Geography*, 44, 155–166, <https://doi.org/10.1080/1088937X.2021.1988001>, 2021.
- 769
- 770 Nossov, D. R., Torre Jorgenson, M., Kielland, K., and Kanevskiy, M. Z.: Edaphic and microclimatic controls over permafrost
771 response to fire in interior Alaska, *Environ. Res. Lett.*, 8, 035013, <https://doi.org/10.1088/1748-9326/8/3/035013>, 2013.
- 772
- 773 O'Donnell, J. A., Harden, J. W., and Manies, K. L.: Soil physical, chemical, and gas flux characterization from *Picea mariana*
774 stands near Erickson Creek, Alaska., U.S. Geological Survey, 2011a.
- 775
- 776 O'Donnell, J. A., Harden, J. W., Manies, K. L., Jorgenson, M. T., and Kanevskiy, M. Z.: Soil data from fire and permafrost-
777 thaw chronosequences in upland *Picea mariana* stands near Hess Creek and Tok, Alaska., US Geological Survey, 2013.
- 778
- 779 O'Donnell, J. A., Harden, J. W., McGUIRE, A. D., Kanevskiy, M. Z., Jorgenson, M. T., and Xu, X.: The effect of fire and
780 permafrost interactions on soil carbon accumulation in an upland black spruce ecosystem of interior Alaska, *Global Change*
781 *Biology*, 17, 1461–1474, <https://doi.org/10.1111/j.1365-2486.2010.02358.x>, 2011b.



- 782
783 O'Donnell, J. A., Harden, J. W., McGuire, A. D., and Romanovsky, V. E.: Exploring the sensitivity of soil carbon dynamics
784 to climate change, fire disturbance and permafrost thaw in a black spruce ecosystem, *Biogeosciences*, 8, 1367–1382,
785 <https://doi.org/10.5194/bg-8-1367-2011>, 2011c.
786
787 Osterkamp, T. E.: Freezing and thawing of soils and permafrost containing unfrozen water or brine, *Water Resources Research*,
788 23, 2279–2285, <https://doi.org/10.1029/WR023i012p02279>, 1987.
789
790 Osterkamp, T. E. and Burn, C. R.: Permafrost, in: *Encyclopedia of Atmospheric Sciences*, Academic Press, 2002.
791
792 Peng, X., Zhang, T., Frauenfeld, O. W., Mu, C., Wang, K., Wu, X., Guo, D., Luo, J., Hjort, J., Aalto, J., Karjalainen, O., and
793 Luoto, M.: Active Layer Thickness and Permafrost Area Projections for the 21st Century, *Earth's Future*, 11, e2023EF003573,
794 <https://doi.org/10.1029/2023EF003573>, 2023.
795
796 Phillips, C. A., Rogers, B. M., Elder, M., Cooperdock, S., Moubarak, M., Randerson, J. T., and Frumhoff, P. C.: Escalating
797 carbon emissions from North American boreal forest wildfires and the climate mitigation potential of fire management, *Sci.*
798 *Adv.*, 8, eabl7161, <https://doi.org/10.1126/sciadv.abl7161>, 2022.
799
800 Rantanen, M., Kämäräinen, M., Niittynen, P., Phoenix, G. K., Lenoir, J., Maclean, I., Luoto, M., and Aalto, J.: Bioclimatic
801 atlas of the terrestrial Arctic, *Sci Data*, 10, 40, <https://doi.org/10.1038/s41597-023-01959-w>, 2023.
802
803 Rocha, A. V., Loranty, M. M., Higuera, P. E., Mack, M. C., Hu, F. S., Jones, B. M., Breen, A. L., Rastetter, E. B., Goetz, S.
804 J., and Shaver, G. R.: The footprint of Alaskan tundra fires during the past half-century: implications for surface properties
805 and radiative forcing, *Environ. Res. Lett.*, 7, 044039, <https://doi.org/10.1088/1748-9326/7/4/044039>, 2012.
806
807 Rocha, A. V. and Shaver, G. R.: Postfire energy exchange in arctic tundra: the importance and climatic implications of burn
808 severity, *Global Change Biology*, 17, 2831–2841, <https://doi.org/10.1111/j.1365-2486.2011.02441.x>, 2011.
809
810 Romanovsky, V. E. and Osterkamp, T. E.: Effects of unfrozen water on heat and mass transport processes in the active layer
811 and permafrost, *Permafrost Periglac. Process.*, 11, 219–239, [https://doi.org/10.1002/1099-1530\(200007/09\)11:3<219::AID-
812 PPP352>3.0.CO;2-7](https://doi.org/10.1002/1099-1530(200007/09)11:3<219::AID-PPP352>3.0.CO;2-7), 2000.
813
814



- 815 Romanovsky, V. E., Smith, S. L., and Christiansen, H. H.: Permafrost thermal state in the polar Northern Hemisphere during
816 the international polar year 2007–2009: a synthesis, *Permafrost & Periglacial*, 21, 106–116, <https://doi.org/10.1002/ppp.689>,
817 2010.
- 818
- 819 Rouse, W. R.: Microclimatic Changes Accompanying Burning in Subarctic Lichen Woodland, *Arctic and Alpine Research*, 8,
820 357, <https://doi.org/10.2307/1550439>, 1976.
- 821
- 822 Rudy, A. C. A., Lamoureux, S. F., Treitz, P., Ewijk, K. V., Bonnaventure, P. P., and Budkewitsch, P.: Terrain Controls and
823 Landscape-Scale Susceptibility Modelling of Active-Layer Detachments, Sabine Peninsula, Melville Island, Nunavut:
824 Landscape-Scale Modelling of Active-Layer Detachment Susceptibility, *Permafrost and Periglac. Process.*, 28, 79–91,
825 <https://doi.org/10.1002/ppp.1900>, 2017.
- 826
- 827 Sannel, A. B. K. and Kuhry, P.: Warming-induced destabilization of peat plateau/thermokarst lake complexes, *J. Geophys.*
828 *Res.*, 116, G03035, <https://doi.org/10.1029/2010JG001635>, 2011.
- 829
- 830 Schädel, C., Rogers, B. M., Lawrence, D. M., Koven, C. D., Brovkin, V., Burke, E. J., Genet, H., Huntzinger, D. N., Jafarov,
831 E., McGuire, A. D., Riley, W. J., and Natali, S. M.: Earth system models must include permafrost carbon processes, *Nat. Clim.*
832 *Chang.*, <https://doi.org/10.1038/s41558-023-01909-9>, 2024.
- 833
- 834 Schaefer, K., Lantuit, H., Romanovsky, V. E., Schuur, E. A. G., and Witt, R.: The impact of the permafrost carbon feedback
835 on global climate, *Environ. Res. Lett.*, 9, 085003, <https://doi.org/10.1088/1748-9326/9/8/085003>, 2014.
- 836
- 837 Scholten, R. C., Coumou, D., Luo, F., and Veraverbeke, S.: Early snowmelt and polar jet dynamics co-influence recent extreme
838 Siberian fire seasons, *Science*, 378, 1005–1009, <https://doi.org/10.1126/science.abn4419>, 2022.
- 839
- 840 Schuur, E. A. G., McGuire, A. D., Schädel, C., Grosse, G., Harden, J. W., Hayes, D. J., Hugelius, G., Koven, C. D., Kuhry,
841 P., Lawrence, D. M., Natali, S. M., Olefeldt, D., Romanovsky, V. E., Schaefer, K., Turetsky, M. R., Treat, C. C., and Vonk, J.
842 E.: Climate change and the permafrost carbon feedback, *Nature*, 520, 171–179, <https://doi.org/10.1038/nature14338>, 2015.
- 843
- 844 Schuur, E. A. G., Abbott, B. W., Commane, R., Ernakovich, J., Euskirchen, E., Hugelius, G., Grosse, G., Jones, M., Koven,
845 C., Leshyk, V., Lawrence, D., Lorant, M. M., Mauritz, M., Olefeldt, D., Natali, S., Rodenhizer, H., Salmon, V., Schädel, C.,
846 Strauss, J., Treat, C., and Turetsky, M.: Permafrost and Climate Change: Carbon Cycle Feedbacks From the Warming Arctic,
847 *Annu. Rev. Environ. Resour.*, 47, 343–371, <https://doi.org/10.1146/annurev-environ-012220-011847>, 2022.
- 848



- 849 See, C. R., Virkkala, A.-M., Natali, S. M., Rogers, B. M., Mauritz, M., Biasi, C., Bokhorst, S., Boike, J., Bret-Harte, M. S.,
850 Celis, G., Chae, N., Christensen, T. R., Murner, S. J., Dengel, S., Dolman, H., Edgar, C. W., Elberling, B., Emmerton, C. A.,
851 Euskirchen, E. S., Göckede, M., Grelle, A., Heffernan, L., Helbig, M., Holl, D., Humphreys, E., Iwata, H., Järveoja, J.,
852 Kobayashi, H., Kochendorfer, J., Kolari, P., Kotani, A., Kutzbach, L., Kwon, M. J., Lathrop, E. R., López-Blanco, E.,
853 Mammarella, I., Marushchak, M. E., Mastepanov, M., Matsuura, Y., Merbold, L., Meyer, G., Minions, C., Nilsson, M. B.,
854 Nojeim, J., Oberbauer, S. F., Olefeldt, D., Park, S.-J., Parmentier, F.-J. W., Peichl, M., Peter, D., Petrov, R., Poyatos, R.,
855 Prokushkin, A. S., Quinton, W., Rodenhizer, H., Sachs, T., Savage, K., Schulze, C., Sjögersten, S., Sonnentag, O., St. Louis,
856 V. L., Torn, M. S., Tuittila, E.-S., Ueyama, M., Varlagin, A., Voigt, C., Watts, J. D., Zona, D., Zyryanov, V. I., and Schuur,
857 E. A. G.: Decadal increases in carbon uptake offset by respiratory losses across northern permafrost ecosystems, *Nat. Clim.*
858 *Chang.*, 14, 853–862, <https://doi.org/10.1038/s41558-024-02057-4>, 2024.
- 859
- 860 Shiklomanov, N. I., Streletskiy, D. A., Nelson, F. E., Hollister, R. D., Romanovsky, V. E., Tweedie, C. E., Bockheim, J. G.,
861 and Brown, J.: Decadal variations of active-layer thickness in moisture-controlled landscapes, Barrow, Alaska, *J. Geophys.*
862 *Res.*, 115, G00I04, <https://doi.org/10.1029/2009JG001248>, 2010.
- 863
- 864 Shur, Y., Hinkel, K. M., and Nelson, F. E.: The transient layer: implications for geocryology and climate-change science,
865 *Permafrost & Periglacial*, 16, 5–17, <https://doi.org/10.1002/ppp.518>, 2005.
- 866
- 867 Sizov, O., Soromotin, A., and Brodt, L.: Temperature of the active layer in the forest-tundra zone in the north of Western
868 Siberia (Pangody) forest-tundra zone in the north of Western Siberia, <https://doi.org/10.5281/zenodo.4285650>, 2020.
- 869
- 870 Smith, S. L. and Burgess, M.: Sensitivity of permafrost to climate warming in Canada, Natural Resources Canada, 2004.
- 871
- 872 Smith, S. L., Romanovsky, V. E., Lewkowicz, A. G., Burn, C. R., Allard, M., Clow, G. D., Yoshikawa, K., and Throop, J.:
873 Thermal state of permafrost in North America: a contribution to the international polar year, *Permafrost & Periglacial*, 21,
874 117–135, <https://doi.org/10.1002/ppp.690>, 2010.
- 875
- 876 Smith, S. L., Riseborough, D. W., and Bonnaventure, P. P.: Eighteen Year Record of Forest Fire Effects on Ground Thermal
877 Regimes and Permafrost in the Central Mackenzie Valley, NWT, Canada, *Permafrost & Periglacial*, 26, 289–303,
878 <https://doi.org/10.1002/ppp.1849>, 2015.
- 879
- 880 Strauss, J., Laboor, S., Schirrmeister, L., Fedorov, A. N., Fortier, D., Froese, D., Fuchs, M., Günther, F., Grigoriev, M., Harden,
881 J., Hugelius, G., Jongejans, L. L., Kanevskiy, M., Kholodov, A., Kunitsky, V., Kraev, G., Lozhkin, A., Rivkina, E., Shur, Y.,
882 Siegert, C., Spektor, V., Streletskaya, I., Ulrich, M., Vartanyan, S., Veremeeva, A., Anthony, K. W., Wetterich, S., Zimov, N.,



- 883 and Grosse, G.: Circum-Arctic Map of the Yedoma Permafrost Domain, *Front. Earth Sci.*, 9, 758360,
884 <https://doi.org/10.3389/feart.2021.758360>, 2021.
- 885
- 886 Streletskiy, D. A., Suter, L. J., Shiklomanov, N. I., Porfiriev, B. N., and Eliseev, D. O.: Assessment of climate change impacts
887 on buildings, structures and infrastructure in the Russian regions on permafrost, *Environ. Res. Lett.*, 14, 025003,
888 <https://doi.org/10.1088/1748-9326/aaf5e6>, 2019.
- 889
- 890 Talucci, A., Loranty, M., Holloway, J., Rogers, B., Alexander, H., Baillargeon, N., Baltzer, J., Berner, L., Breen, A., Brodt,
891 L., Buma, B., Delcourt, C., Diaz, L., Dieleman, C., Douglas, T., Frost, G., Gaglioti, B., Hewitt, R., Hollingsworth, T.,
892 Jorgenson, M. T., Lara, M., Loehman, R., Mack, M., Manies, K., Minions, C., Natali, S., O'Donnell, J., Olefeldt, D., Paulson,
893 A., Rocha, A., Saperstein, L., Shestakova, T., Sistla, S., Oleg, S., Soromotin, A., Turetsky, M., Veraverbeke, S., and Walvoord,
894 M.: FireALT dataset: estimated active layer thickness for paired burned unburned sites measured from 2001-2023,
895 <https://doi.org/10.18739/A2W950Q33>, 2024.
- 896
- 897 Treharne, R., Rogers, B. M., Gasser, T., MacDonald, E., and Natali, S.: Identifying Barriers to Estimating Carbon Release
898 From Interacting Feedbacks in a Warming Arctic, *Front. Clim.*, 3, 716464, <https://doi.org/10.3389/fclim.2021.716464>, 2022.
- 899
- 900 Turetsky, M. R., Abbott, B. W., Jones, M. C., Anthony, K. W., Olefeldt, D., Schuur, E. A. G., Grosse, G., Kuhry, P., Hugelius,
901 G., Koven, C., Lawrence, D. M., Gibson, C., Sannel, A. B. K., and McGuire, A. D.: Carbon release through abrupt permafrost
902 thaw, *Nat. Geosci.*, 13, 138–143, <https://doi.org/10.1038/s41561-019-0526-0>, 2020.
- 903
- 904 Wang, Z., Schaaf, C. B., Chopping, M. J., Strahler, A. H., Wang, J., Román, M. O., Rocha, A. V., Woodcock, C. E., and Shuai,
905 Y.: Evaluation of Moderate-resolution Imaging Spectroradiometer (MODIS) snow albedo product (MCD43A) over tundra,
906 *Remote Sensing of Environment*, 117, 264–280, <https://doi.org/10.1016/j.rse.2011.10.002>, 2012.
- 907
- 908 Wotton, B. M., Flannigan, M. D., and Marshall, G. A.: Potential climate change impacts on fire intensity and key wildfire
909 suppression thresholds in Canada, *Environ. Res. Lett.*, 12, 095003, <https://doi.org/10.1088/1748-9326/aa7e6e>, 2017.
- 910
- 911 Yokohata, T., Saito, K., Ito, A., Ohno, H., Tanaka, K., Hajima, T., and Iwahana, G.: Future projection of greenhouse gas
912 emissions due to permafrost degradation using a simple numerical scheme with a global land surface model, *Prog Earth Planet
913 Sci*, 7, 56, <https://doi.org/10.1186/s40645-020-00366-8>, 2020.
- 914
- 915 York, A., Bhatt, U. S., Gargulinski, E., Grabinski, Z., Jain, P., Soja, A., Thoman, R. L., Ziel, R., Alaska Center for Climate
916 Assessment and Policy (U.S.), International Arctic Research Center, United States. National Oceanic and Atmospheric
917 Administration. Office of Oceanic and Atmospheric Research, and Cooperative Institute for Research in the Atmosphere (Fort



- 918 Collins, Colo.): Arctic Report Card 2020: Wildland Fire in High Northern Latitudes, <https://doi.org/10.25923/2GEF-3964>,
919 2020.
920
- 921 Zhang, Y., Chen, W., and Riseborough, D. W.: Transient projections of permafrost distribution in Canada during the 21st
922 century under scenarios of climate change, *Global and Planetary Change*, 60, 443–456,
923 <https://doi.org/10.1016/j.gloplacha.2007.05.003>, 2008.
924
- 925 Zhang, Y., Wolfe, S. A., Morse, P. D., Olthof, I., and Fraser, R. H.: Spatiotemporal impacts of wildfire and climate warming
926 on permafrost across a subarctic region, Canada, *JGR Earth Surface*, 120, 2338–2356, <https://doi.org/10.1002/2015JF003679>,
927 2015.
928
- 929 Zheng, B., Ciais, P., Chevallier, F., Yang, H., Canadell, J. G., Chen, Y., Van Der Velde, I. R., Aben, I., Chuvieco, E., Davis,
930 S. J., Deeter, M., Hong, C., Kong, Y., Li, H., Li, H., Lin, X., He, K., and Zhang, Q.: Record-high CO₂ emissions from boreal
931 fires in 2021, *Science*, 379, 912–917, <https://doi.org/10.1126/science.ade0805>, 2023.
932